Ezh2 loss propagates hypermethylation at T cell differentiation–regulating genes to promote leukemic transformation

Changshan Wang,[1,2] Motohiko Oshima,[2] Daisuke Sato,[2] Hirotaka Matsui,[3] Sho Kubota,[4] Kazumasa Aoyama,[2] Yaeko Nakajima-Takagi,[2] Shuhei Koide,[2] Jun Matsubayashi,[5] Makiko Mochizuki-Kashio,[2] Takako Nakano-Yokomizo,[4] Jie Bai,[4] Toshitaka Nagao,[5] Akinori Kanai,[6] Atsushi Iwama,[2,7] and Goro Sashida[2,4]

[1]The State Key Laboratory of Reproductive Regulation and Breeding of Grassland Livestock, School of Life Sciences, Inner Mongolia University, Hohhot, China. [2]Department of Cellular and Molecular Medicine, Graduate School of Medicine, Chiba University, Chiba, Japan. [3]Department of Molecular Laboratory Medicine, Faculty of Life Sciences, and [4]Laboratory of Transcriptional Regulation in Leukemogenesis, International Research Center for Medical Sciences, Kumamoto University, Kumamoto, Japan. [5]Department of Anatomic Pathology, Tokyo Medical University, Tokyo, Japan. [6]Department of Molecular Oncology, Research Institute for Radiation Biology and Medicine, Hiroshima University, Hiroshima, Japan. [7]Division of Stem Cell and Molecular Medicine, Center for Stem Cell Biology and Regenerative Medicine, Institute of Medical Science, University of Tokyo, Tokyo, Japan.

Early T cell precursor acute lymphoblastic leukemia (ETP-ALL) is a new pathological entity with poor outcomes in T cell ALL (T-ALL) that is characterized by a high incidence of loss-of-function mutations in polycomb repressive complex 2 (PRC2) genes. We generated a mouse model of ETP-ALL by deleting *Ezh2*, one of the PRC2 genes, in *p53*-null hematopoietic cells. The loss of Ezh2 in *p53*-null hematopoietic cells impeded the differentiation of ETPs and eventually induced ETP-ALL–like disease in mice, indicating that PRC2 functions as a bona fide tumor suppressor in ETPs. A large portion of PRC2 target genes acquired DNA hypermethylation of their promoters following reductions in H3K27me3 levels upon the loss of Ezh2, which included pivotal T cell differentiation–regulating genes. The reactivation of a set of regulators by a DNA-demethylating agent, but not the transduction of single regulator genes, effectively induced the differentiation of ETP-ALL cells. Thus, PRC2 protects key T cell developmental regulators from DNA hypermethylation in order to keep them primed for activation upon subsequent differentiation phases, while its insufficiency predisposes ETPs to leukemic transformation. These results revealed a previously unrecognized epigenetic switch in response to PRC2 dysfunction and provide the basis for specific rational epigenetic therapy for ETP-ALL with PRC2 insufficiency.

Introduction

Early T cell precursor acute lymphoblastic leukemia (ETP-ALL) has been identified as a new pathological entity of T cell ALL (T-ALL) that shows resistance to conventional chemotherapies and has a poor outcome (1). Normal ETPs are a subset of recent immigrants from BM to the thymus and retain the ability to differentiate into T cells and myeloid cells, but not B cells. ETP-ALL cells lack mature T cell–lineage markers, such as CD1a and CD8, but show the aberrant expression of surface markers for hematopoietic stem cells (HSCs) and myeloid cells (e.g., c-Kit, CD13, CD33) (1). In contrast to cortical T-ALL characterized by the activation of *NOTCH1* mutations, ETP-ALL has been characterized by the activation of mutations in genes encoding cytokine receptors and RAS signaling molecules (e.g., *IL7R* and *NRAS*) as well as inactivating mutations in polycomb repressive complex 2 (PRC2) genes (2).

PRC2 consists of EZH2, EED, and SUZ12. EZH2 is an enzymatic component of PRC2 that catalyzes the trimethylation of histone H3 at lysine 27 (H3K27me3) and maintains the silencing of critical genes for differentiation in hematopoiesis (3, 4). Loss-of-function mutations in *EZH2* were initially identified in patients with clonal myeloid malignancies originating from HSCs, such as myelodysplastic syndrome (MDS), myeloproliferative neoplasm (MPN), and MDS/MPN overlap disorders (5, 6). Deletions and/or loss-of-function mutations in PRC2 genes were subsequently identified at high frequencies in patients with ETP-ALL (16% *EZH2*, 17% *SUZ12*, and 13% *EED*) and non-ETP T-ALL patients (5%–16% *EZH2* and 2%–4% *SUZ12*) (2, 7). We previously demonstrated that the hematopoietic cell–specific deletion of *Ezh2* collaborated with *Tet2* loss, *RUNX1* mutants, or the $JAK2^{V671F}$ mutant in the development of myeloid malignancies in mice (8–10). We and others also reported that the absence of *Ezh2* alone also induced non-ETP T-ALL in mice (11, 12). These findings indicate that Ezh2 functions as a tumor suppressor, not only in myeloid malignancies, but also in T cell malignancies, including ETP-ALL.

In order to examine how PRC2 inactivation promotes the development of ETP-ALL in vivo, an ETP-ALL mouse model has been developed using hematopoietic progenitors deficient for *Cdkn2a* and *Eed* or *Ezh2*, which were transformed by $NRAS^{Q61K}$ on OP9-DLL1, a stromal cell line expressing the Notch ligand delta-like 1 (DLL1). The transformed cells induced ETP-ALL–like leukemia with a double-negative 1 thymocyte (DN1) ($CD44^+CD25^-$) and DN2 ($CD44^+CD25^+$) surface phenotype in recipient mice (13). However, additional models that precisely recapitulate the

Conflict of interest: The authors have declared that no conflict of interest exists.
Submitted: April 18, 2017; **Accepted:** June 19, 2018.
Reference information: *J Clin Invest*. 2018;128(9):3872–3886.
https://doi.org/10.1172/JCI94645.

phenotypic and transcriptional features of human ETP-ALL are needed in order to understand the impact of PRC2 inactivation in the pathogenesis of ETP-ALL. In the present study, we generated a mouse model of ETP-ALL by deleting *Ezh2* and *p53* in mice. We found that *Ezh2p53*-deficient mice preferentially developed lethal T-ALL compatible with human ETP-ALL rather than thymic lymphoma, which typically develops in *p53*-deficient mice (14).

We herein demonstrate how the loss of Ezh2 induced an epigenetic switch from a H3K27me3 modification to DNA hypermethylation at CpG island (CGI) promoter regions in thymic precursor cells, leading to the suppressed expression of critical T cell commitment regulators, such as *Runx1* and *Bcl11b*, but the sustained expression of HSC signature genes, thereby promoting the transformation of ETP-ALL. We also provide evidence for the greater sensitivity of *Ezh2p53*-deficient ETP-ALL cells to decitabine (DAC), a DNA-demethylating agent, which restored the differentiation of ETP-ALL cells. Our results indicate that Ezh2-PRC2 protects key T cell developmental regulator genes from DNA hypermethylation in order to keep them primed for activation upon subsequent differentiation phases; however, its disruption initiates the transformation of immature T cell leukemia.

Results

Ezh2 loss causes lethal hematological malignancies in the absence of p53. Since deletions and loss-of-function mutations in PRC2 genes, including *EZH2*, have frequently been observed in patients with ETP-ALL, we attempted to establish whether the deletion of *Ezh2* promotes the development of ETP-ALL in vivo. The p53 pathway is often inactivated in patients with ETP-ALL via genetic deletions or mutations of *CDKN2A* (2, 15). In addition, mutations in both *p53* and *SUZ12*, a PRC2 gene, were found in a patient with ETP-ALL (16). These findings prompted us to combine PRC2 and p53 insufficiency to accelerate the development of ETP-ALL. We generated *Ezh2$^{fl/fl}$;p53$^{fl/fl}$;Cre-ERT2* compound mice. Total BM cells isolated from *Cre-ERT2*, *Ezh2$^{fl/fl}$;Cre-ERT2*, *p53$^{fl/fl}$;Cre-ERT2*, and *Ezh2$^{fl/fl}$;p53$^{fl/fl}$;Cre-ERT2* mice were transplanted into lethally irradiated CD45.1$^+$ WT recipient mice. We then deleted *Ezh2* and/or *p53* by activating Cre recombinase via intraperitoneal injections of tamoxifen at 4 weeks after transplantation (Figure 1A). We hereafter refer to recipient mice reconstituted with WT, *Ezh2$^{\Delta/\Delta}$*, *p53$^{\Delta/\Delta}$*, and *Ezh2$^{\Delta/\Delta}$p53$^{\Delta/\Delta}$* BM cells as WT, Ezh2$^{\Delta/\Delta}$, p53$^{\Delta/\Delta}$, and Ezh2$^{\Delta/\Delta}$p53$^{\Delta/\Delta}$ mice. We confirmed the successful abolishment of *Ezh2* and *p53* transcripts (Figure 1B) and decreased H3K27me3 levels (Figure 1C) in CD4$^-$CD8$^-$ DN thymocytes isolated from Ezh2$^{\Delta/\Delta}$p53$^{\Delta/\Delta}$ mice.

Ezh2$^{\Delta/\Delta}$ mice showed leukopenia due to impaired B lymphopoiesis and variable platelet counts in peripheral blood (PB) at 3 months after transplantation (Figure 1, D and E) and developed myeloid malignancies, including MDS and MDS/MPN, but not T cell malignancies in the primary recipients (median survival, 327.5 days), as we previously reported (8, 11). While p53$^{\Delta/\Delta}$ mice did not show significant changes in blood cell counts at 3 months after transplantation, they died by 6 months after transplantation, with a markedly enlarged thymus due to the expansion of CD3$^+$CD4$^{+/-}$CD8$^+$TCR-β$^+$ tumor cells (Figure 1, F–H), which is compatible with thymic lymphoma, as previously reported (14, 17). In contrast, Ezh2$^{\Delta/\Delta}$p53$^{\Delta/\Delta}$ mice showed progressive anemia and severe leukopenia accompanied by the emergence of immature blasts in PB (Figure 1, D and E) and died by 8 months after transplantation with a longer latency than p53$^{\Delta/\Delta}$ mice (median survival, 189 days versus 137 days, $P < 0.0001$) (Figure 1I). We observed similar survival outcomes for Ezh2$^{\Delta/\Delta}$p53$^{\Delta/\Delta}$ mice in 3 independent cohorts (data not shown). Taken together, the loss of Ezh2 and p53 cooperatively impaired hematopoiesis and promoted the development of a lethal hematological disease.

Ezh2 loss promotes the development of ETP-ALL in the absence of p53. The accumulation of CD8$^+$ single-positive (SP) cells in the thymus was evident in p53$^{\Delta/\Delta}$ mice (Figure 2, A and B) at 3 months after transplantation, prior to the emergence of lethal disease. In contrast, Ezh2$^{\Delta/\Delta}$ mice and Ezh2$^{\Delta/\Delta}$p53$^{\Delta/\Delta}$ mice showed a significant increase in the proportion of CD4$^-$CD8$^-$ (DN) T cells (Figure 2, A and B), particularly DN2 cells (Figure 2, C and D). These results indicate that the loss of Ezh2 impaired T cell differentiation at the DN2 to DN3 transition. Ezh2$^{\Delta/\Delta}$p53$^{\Delta/\Delta}$ mice eventually developed lethal disease, with a significantly enlarged thymus and spleen (Figure 2, E and F). A detailed analysis of moribund Ezh2$^{\Delta/\Delta}$p53$^{\Delta/\Delta}$ mice revealed the expansion of leukemic blasts with a high nucleocytoplasmic ratio in the thymus in 15 out of 18 Ezh2$^{\Delta/\Delta}$p53$^{\Delta/\Delta}$ mice (Figure 2G), which showed a CD4$^{-/mid}$CD8$^-$c-Kit$^+$ immunophenotype with DN1- (CD44$^+$CD25$^-$), DN2- (CD44$^+$CD25$^+$), or DN1/2-like (CD44$^+$CD25$^{-/+}$) features (Figure 2, H and I). A flow cytometric analysis identified cytoplasmic CD3 (cyCD3) in these leukemic cells (data not shown), and a histological analysis also detected the expression of cytoplasmic CD3 (Figure 2J), consistent with the immature phenotypic hallmarks of human ETP-ALL (1). These leukemic cells massively infiltrated the spleen and liver tissues (Figure 2J) as well as PB (Figure 1E), indicating that Ezh2$^{\Delta/\Delta}$p53$^{\Delta/\Delta}$ mice preferentially developed aggressive ETP-ALL. We also identified a monoclonal rearrangement of the TCR-β loci in Ezh2$^{\Delta/\Delta}$p53$^{\Delta/\Delta}$ leukemic DN cells, indicating the thymus origin of Ezh2$^{\Delta/\Delta}$p53$^{\Delta/\Delta}$ ETP-ALL (Figure 2K). In contrast to Ezh2$^{\Delta/\Delta}$ mice, which developed MDS and MDS/MPN after a long latency, Ezh2$^{\Delta/\Delta}$p53$^{\Delta/\Delta}$ mice died of ETP-ALL much earlier than Ezh2$^{\Delta/\Delta}$ mice (Figure 1I). BM analysis revealed only mild changes in the proportions of stem cells/myeloid progenitors and myeloid cells in Ezh2$^{\Delta/\Delta}$p53$^{\Delta/\Delta}$ mice (Supplemental Figure 1; supplemental material available online with this article; https://doi.org/10.1172/JCI94645DS1), indicating that Ezh2$^{\Delta/\Delta}$p53$^{\Delta/\Delta}$ mice did not have apparent myeloid malignancies.

We next transplanted either BM cells or thymocyte cells (1×10^6 cells) isolated from Ezh2$^{\Delta/\Delta}$p53$^{\Delta/\Delta}$ ETP-ALL mice into sublethally irradiated secondary recipients. All of the secondary recipients developed lethal ETP-ALL in a manner similar to the primary recipients and showed severe anemia and thrombocytopenia (Supplemental Figure 2). The secondary recipients showed obviously shorter survival than did the primary Ezh2$^{\Delta/\Delta}$p53$^{\Delta/\Delta}$ mice (Figure 1I and Supplemental Figure 3). Although 3 out of 18 Ezh2$^{\Delta/\Delta}$p53$^{\Delta/\Delta}$ mice developed more differentiated CD8$^+$TCR-β$^+$ thymic lymphoma (Figure 2H), similarly to p53$^{\Delta/\Delta}$ mice, these results indicate that the loss of *Ezh2* facilitates the development of progressive ETP-ALL in mice lacking *p53*.

The loss of Ezh2 impedes T cell differentiation at the CD4$^-$CD8$^-$ stage. In order to understand the differentiation properties of Ezh2$^{\Delta/\Delta}$p53$^{\Delta/\Delta}$ thymocytes, we cultured CD44$^+$CD25$^-$ DN1 cells isolated

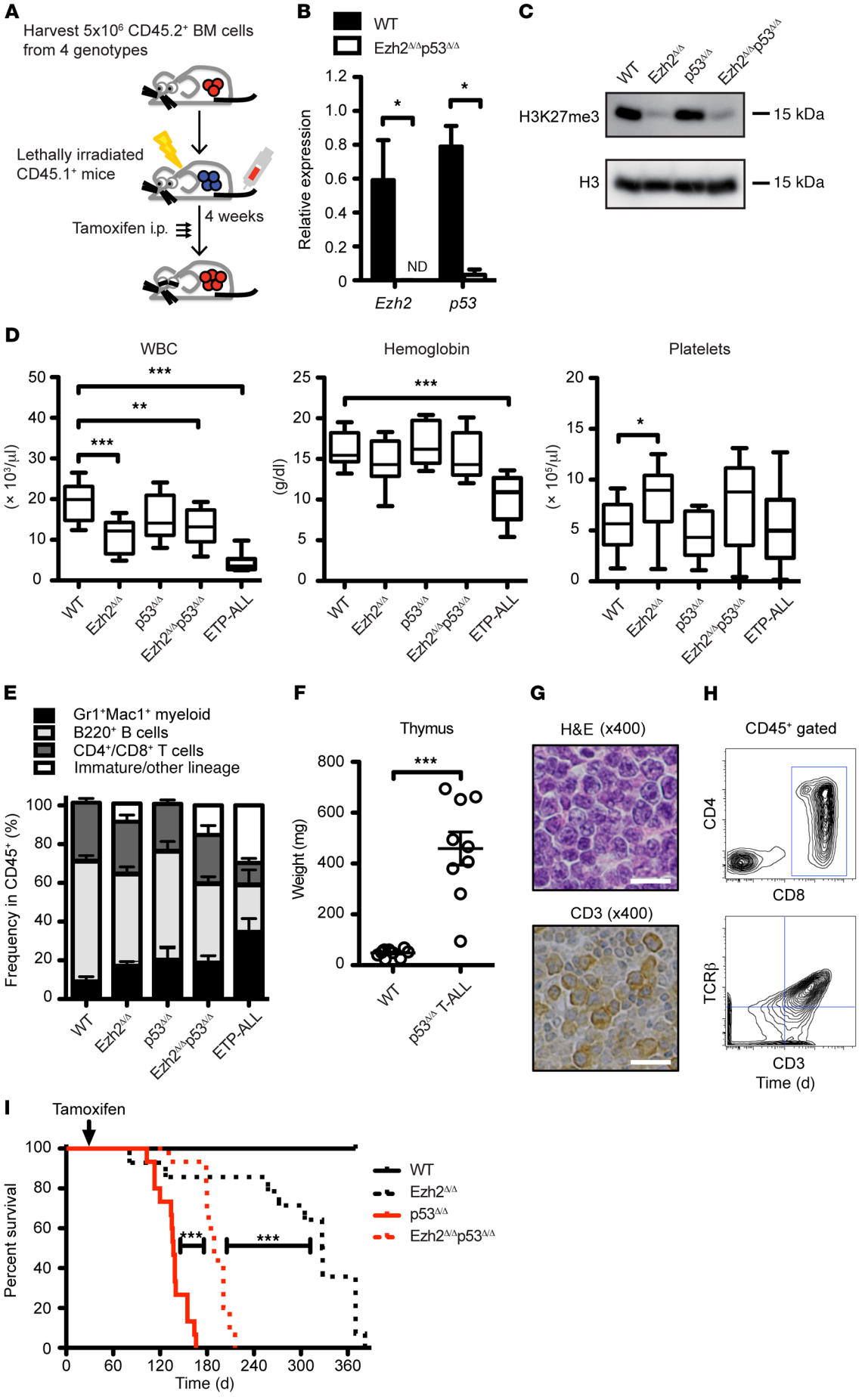
A
Harvest 5x10⁶ CD45.2⁺ BM cells from 4 genotypes
Lethally irradiated CD45.1⁺ mice
Tamoxifen i.p.
4 weeks
B
WT
Ezh2ΔΔp53ΔΔ
Relative expression
ND
Ezh2
p53
C
WT
Ezh2ΔΔ
p53ΔΔ
Ezh2ΔΔp53ΔΔ
H3K27me3
H3
15 kDa
D
WBC
Hemoglobin
Platelets
(× 10³/μl)
(g/dl)
(× 10⁵/μl)
WT
Ezh2ΔΔ
p53ΔΔ
Ezh2ΔΔp53ΔΔ
ETP-ALL
E
Gr1⁺Mac1⁺ myeloid
B220⁺ B cells
CD4⁺/CD8⁺ T cells
Immature/other lineage
Frequency in CD45⁺ (%)
F
Thymus
Weight (mg)
p53ΔΔ T-ALL
G
H&E (x400)
CD3 (x400)
H
CD45⁺ gated
CD4
CD8
TCRβ
CD3
I
Tamoxifen
Percent survival
Time (d)

Figure 1. Ezh2 loss impaired hematopoiesis and caused lethal disease in the absence of p53. (**A**) Experimental schematic of our mouse model utilizing *Ezh2* and/or *p53* conditional knockout BM cells transplanted into lethally irradiated WT CD45.1$^+$ recipients. (**B**) Quantitative RT-PCR analysis of the expression of *Ezh2* and *p53* in CD44$^+$CD25$^-$CD4$^-$CD8$^-$ (DN1) cells from WT (n = 4) and Ezh2$^{\Delta/\Delta}$p53$^{\Delta/\Delta}$ mice (n = 4) 4 weeks after the deletion of *Ezh2* and *p53*. *Gapdh* was used to normalize the amount of input RNA. Data are shown as mean ± SD. *P < 0.05, Mann-Whitney U test. N.D., not determined. (**C**) Verification of H3K27me3 levels in CD4$^-$CD8$^-$ (DN) cells from WT, Ezh2$^{\Delta/\Delta}$, p53$^{\Delta/\Delta}$, and Ezh2$^{\Delta/\Delta}$p53$^{\Delta/\Delta}$ mice examined by Western blotting. Histone H3 was used as a loading control. (**D**) Complete blood cell counts of WT (n = 10), Ezh2$^{\Delta/\Delta}$ (n = 13), p53$^{\Delta/\Delta}$ (n = 15), and Ezh2$^{\Delta/\Delta}$ p53$^{\Delta/\Delta}$ (n = 14) mice 3 months after transplantation and moribund Ezh2$^{\Delta/\Delta}$ p53$^{\Delta/\Delta}$ ETP-ALL mice (n = 11) at the time of sacrifice. Data are shown as box-and-whiskers plots drawing minimum to maximum. *P < 0.05; **P < 0.01; ***P < 0.001, Student's t test. (**E**) Proportions of myeloid (Gr-1$^+$ and/or Mac-1$^+$), B220$^+$ B cells, CD4$^+$ or CD8$^+$ T cells, and immature cells negative for these surface markers among CD45.2$^+$ donor-derived hematopoietic cells in PB. Data are shown as mean ± SEM (n = 10–15). (**F**) Thymus weight of WT mice (n = 10) 3 months after transplantation and p53$^{\Delta/\Delta}$ T-ALL mice (n = 9) at the time of sacrifice. Data are shown as mean ± SEM. ***P < 0.001, Mann-Whitney U test. (**G**) Histology of the thymus of a p53$^{\Delta/\Delta}$ T-ALL mouse observed by H&E staining (top) and CD3 staining (bottom). Original magnification, ×400. Scale bars: 20 μm. (**H**) Representative flow cytometric profiles of CD45$^+$-gated thymocytes in the thymus of a p53$^{\Delta/\Delta}$ T-ALL mouse shown from **F** (n = 9). (**I**) Kaplan-Meier survival curve. Median survival was significantly shorter in Ezh2$^{\Delta/\Delta}$p53$^{\Delta/\Delta}$ mice (n = 14) than in Ezh2$^{\Delta/\Delta}$ mice (n = 13) (189 days versus 327.5 days), but longer in Ezh2$^{\Delta/\Delta}$p53$^{\Delta/\Delta}$ mice (n = 14) than in p53$^{\Delta/\Delta}$ mice (n = 15) (189 days versus 137 days). ***P < 0.0001, log-rank test.

from the WT, Ezh2$^{\Delta/\Delta}$, p53$^{\Delta/\Delta}$, and Ezh2$^{\Delta/\Delta}$p53$^{\Delta/\Delta}$ thymus on TSt-4/DLL1 stromal cells, which express the Notch ligand DLL1 (Figure 3A). Ezh2$^{\Delta/\Delta}$ DN1 cells did not grow well (Figure 3B), presumably due to the derepression of *p16^{Ink4a}* and *p19^{Arf}* in the culture (11). In contrast, Ezh2$^{\Delta/\Delta}$p53$^{\Delta/\Delta}$ DN1 cells showed significantly better proliferation than WT and p53$^{\Delta/\Delta}$ cells (Figure 3B), suggesting that the deletion of *p53* canceled the impaired growth of Ezh2$^{\Delta/\Delta}$ cells. While WT DN1 cells efficiently generated DP cells (Figure 3, C and D), DN1 cells deficient for *Ezh2* showed significantly impaired differentiation and mostly stayed in the DN1 and DN2 stages, resulting in the massive expansion of Ezh2$^{\Delta/\Delta}$p53$^{\Delta/\Delta}$ DN1/2 cells in the culture (Figure 3, E and F). These results match the behavior of Ezh2$^{\Delta/\Delta}$p53$^{\Delta/\Delta}$ thymocytes in vivo and indicate that the loss of both Ezh2 and p53 cooperates in the expansion of DN1/2 cells.

The loss of Ezh2 and p53 deregulates the transcriptional program of T cell differentiation. In order to understand the molecular mechanisms underlying the pathogenesis of Ezh2$^{\Delta/\Delta}$p53$^{\Delta/\Delta}$ ETP-ALL, we performed gene expression profiling by a microarray analysis in DN1, DN2, and DN3 cells isolated from WT, Ezh2$^{\Delta/\Delta}$, p53$^{\Delta/\Delta}$, and Ezh2$^{\Delta/\Delta}$p53$^{\Delta/\Delta}$ mice at a preleukemic stage and leukemic DN2 cells isolated from 2 Ezh2$^{\Delta/\Delta}$p53$^{\Delta/\Delta}$ mice that developed DN1/2-type ETP-ALL. As expected, hierarchical clustering and a principal component analysis based on the microarray data revealed that the expression profiles of ETP-ALL cells were more similar to those of Ezh2$^{\Delta/\Delta}$p53$^{\Delta/\Delta}$ DN cells than those of Ezh2$^{\Delta/\Delta}$ and p53$^{\Delta/\Delta}$ DN cells (Figure 4, A and B). An integrative analysis revealed a set of 1,664, 2,714, and 2,210 upregulated genes and 1,432, 2,516, and 1,928 downregulated genes in Ezh2$^{\Delta/\Delta}$p53$^{\Delta/\Delta}$ DN2 cells at a preleukemic stage and 2 ETP-ALL cells relative to WT DN2 cells, respectively (Figure 4C), indicating that alterations in gene expression propagated during the development of ETP-ALL. These results indicate that Ezh2$^{\Delta/\Delta}$p53$^{\Delta/\Delta}$ leukemic cells impeded the subsequent operation of T cell development gene networks at the DN2 and DN3 stages, but also underwent an oncogenic transcriptional reprograming that was not seen in the absence of either Ezh2 or p53.

The loss of Ezh2 leads to the silencing of critical T cell–lineage determinants. In order to clarify how the deletion of *Ezh2* altered the transcriptional program of T cell development, we performed ChIP-sequencing (ChIP-seq) of H3K27me3 in DN1 cells isolated from WT, Ezh2$^{\Delta/\Delta}$, p53$^{\Delta/\Delta}$, and Ezh2$^{\Delta/\Delta}$p53$^{\Delta/\Delta}$ mice. We found that H3K27me3 levels at the promoter regions of RefSeq genes were significantly lower in Ezh2$^{\Delta/\Delta}$ cells and Ezh2$^{\Delta/\Delta}$p53$^{\Delta/\Delta}$ cells, but not in p53$^{\Delta/\Delta}$ cells, than in WT cells (Figure 5A). A gene set enrichment analysis (GSEA) revealed that the canonical PRC2 target genes, which were defined by the levels of H3K27me3 in WT DN1 cells (≥2.5-fold enrichment over the input signal) (Supplemental Table 1), were positively enriched in Ezh2$^{\Delta/\Delta}$ DN2 cells and Ezh2$^{\Delta/\Delta}$p53$^{\Delta/\Delta}$ DN2 cells at preleukemic and leukemic stages compared with WT DN2 cells (Figure 5B and Supplemental Figure 4). The enrichment of canonical PRC2 targets was also markedly greater in Ezh2$^{\Delta/\Delta}$ p53$^{\Delta/\Delta}$ DN1 cells than in WT DN1 cells (data not shown). However, we noted that the enrichment of PRC2 targets was slightly blunted in ETP-ALL cells than in preleukemic Ezh2$^{\Delta/\Delta}$p53$^{\Delta/\Delta}$ cells, implying that alternative mechanisms operate to repress the transcription of PRC2 targets during the leukemic transformation.

Among canonical PRC2 targets, the expression of *p16^{Ink4a}* and *p19^{Arf}* was derepressed following the loss of H3K27me3 modifications at the *Cdkn2a* locus in Ezh2$^{\Delta/\Delta}$p53$^{\Delta/\Delta}$ cells (Figure 5C). In contrast, the expression of *Nr4a3/Ncor1*, a target of TCR signaling in DN2 cells (18), was significantly downregulated in Ezh2$^{\Delta/\Delta}$ p53$^{\Delta/\Delta}$ preleukemic and leukemic cells despite the loss of the H3K27me3 mark at its promoter region (Figure 5D). Correspondingly, the repression of a set of genes that are upregulated at the transition from the DN2 to DN3 stages (19) was significantly greater in ETP-ALL leukemic cells than in Ezh2$^{\Delta/\Delta}$p53$^{\Delta/\Delta}$ preleukemic cells (Figure 5E). Among these, the expression of critical T cell development regulators, such as *Runx1*, *Bcl11b*, and *Ptcra*, was specifically repressed in Ezh2$^{\Delta/\Delta}$p53$^{\Delta/\Delta}$ DN2 cells during the development of ETP-ALL (Figure 5F), which is consistent with the perturbed differentiation phenotype of Ezh2$^{\Delta/\Delta}$p53$^{\Delta/\Delta}$ leukemic cells (Figure 3, D and F).

Since *Runx1* and *Bcl11b* are required for T cell commitment and the loss of myeloid potential at the DN2b stage (20, 21), we transduced CD44$^+$CD25$^{-/mid}$ DN1/2 leukemic cells with either *RUNX1* or *Bcl11b* and analyzed their capacity to differentiate in vitro (Figure 5G). While the expression of *Bcl11b* failed to induce the differentiation of leukemic cells beyond the DN3 stage (data not shown), exogenous *RUNX1* significantly promoted the differentiation of leukemic cells to the DN4 stage (Figure 5, H and I). Since *RUNX1* loss-of-function mutations are often found in ETP-ALL patients and are associated with poor clinical outcomes (2, 22), *Runx1* appeared to be one of the tumor suppressor genes inactivated in this context.

The aberrant expression of some HSC and myeloid markers is a hallmark of human ETP-ALL (1, 2). Therefore, we analyzed the expression profiles of Ezh2$^{\Delta/\Delta}$p53$^{\Delta/\Delta}$ ETP-ALL cells by utilizing the gene sets generated from defined murine hematopoietic fractions

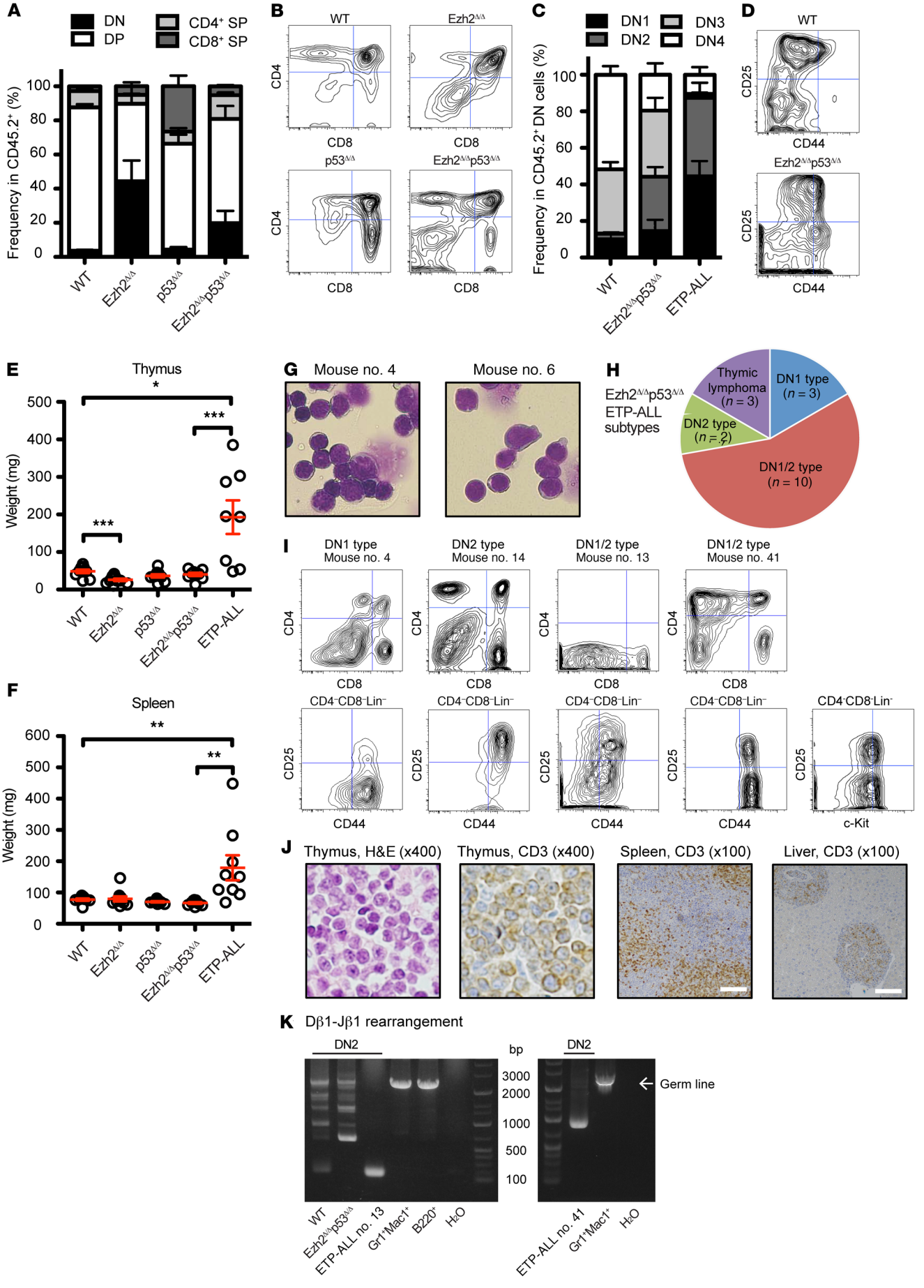
A
DN
DP
CD4+ SP
CD8+ SP
Frequency in CD45.2+ (%)
WT
Ezh2Δ/Δ
p53Δ/Δ
Ezh2Δ/Δp53Δ/Δ
B
WT
Ezh2Δ/Δ
p53Δ/Δ
Ezh2Δ/Δp53Δ/Δ
CD4
CD8
C
DN1
DN2
DN3
DN4
Frequency in CD45.2+DN cells (%)
ETP-ALL
D
CD25
CD44
E
Thymus
Weight (mg)
F
Spleen
G
Mouse no. 4
Mouse no. 6
H
Ezh2Δ/Δp53Δ/Δ ETP-ALL subtypes
Thymic lymphoma (n = 3)
DN1 type (n = 3)
DN2 type (n = 2)
DN1/2 type (n = 10)
I
DN1 type Mouse no. 4
DN2 type Mouse no. 14
DN1/2 type Mouse no. 13
DN1/2 type Mouse no. 41
CD4-CD8-Lin-
c-Kit
J
Thymus, H&E (x400)
Thymus, CD3 (x400)
Spleen, CD3 (x100)
Liver, CD3 (x100)
K
Dβ1-Jβ1 rearrangement
DN2
bp
3000
2000
1000
500
100
Germ line
ETP-ALL no. 13
Gr1+Mac1+
B220+
H2O
ETP-ALL no. 41

Figure 2. Ezh2 loss promoted the development of ETP-ALL in the absence of p53. (**A**) Proportions of $CD4^-CD8^-$ DN cells among $CD45.2^+$ cells in the thymus of WT, $Ezh2^{\Delta/\Delta}$, $p53^{\Delta/\Delta}$, and $Ezh2^{\Delta/\Delta}p53^{\Delta/\Delta}$ (n = 4–7) mice 3 months after transplantation. Data are shown as mean ± SEM. (**B**) Representative flow cytometric profiles of CD4 and CD8 expression on donor-derived $CD45.2^+$ cells in the thymus of WT, $Ezh2^{\Delta/\Delta}$, $p53^{\Delta/\Delta}$, and $Ezh2^{\Delta/\Delta}p53^{\Delta/\Delta}$ mice. (**C**) Proportions of $CD44^+CD25^-$ DN1, $CD44^+CD25^+$ DN2, $CD44^-CD25^+$ DN3, and $CD44^-CD25^-$ DN4 cells among donor-derived $CD45.2^+CD4^-CD8^-$ DN cells in the thymus (n = 4–7). Data are shown as mean ± SEM. (**D**) Representative flow cytometric profiles of CD44 and CD25 expression on $CD45.2^+$ DN cells in the thymus of WT and $Ezh2^{\Delta/\Delta}p53^{\Delta/\Delta}$ mice. (**E**) Thymus weight of WT (n = 10), $Ezh2^{\Delta/\Delta}$ (n = 10), $p53^{\Delta/\Delta}$ (n = 10), and $Ezh2^{\Delta/\Delta}p53^{\Delta/\Delta}$ (n = 9) mice 3 months after transplantation and moribund $Ezh2^{\Delta/\Delta}p53^{\Delta/\Delta}$ ETP-ALL mice (n = 8) at the time of sacrifice. Data are shown as mean ± SEM. $^*P < 0.05$; $^{***}P < 0.001$, Student's t test (WT vs. $Ezh2^{\Delta/\Delta}$) or Mann-Whitney U test (WT vs. ETP-ALL and $Ezh2^{\Delta/\Delta}p53^{\Delta/\Delta}$ vs. ETP-ALL). (**F**) Spleen weight of WT (n = 10), $Ezh2^{\Delta/\Delta}$ (n = 10), $p53^{\Delta/\Delta}$ (n = 10), and $Ezh2^{\Delta/\Delta}p53^{\Delta/\Delta}$ (n = 9) mice 3 months after transplantation and moribund $Ezh2^{\Delta/\Delta}p53^{\Delta/\Delta}$ ETP-ALL mice (n = 8) at the time of sacrifice. Data are shown as mean ± SEM. $^{**}P < 0.01$, Mann-Whitney U test. (**G**) Immature leukemic cells in the thymus of $Ezh2^{\Delta/\Delta}p53^{\Delta/\Delta}$ ETP-ALL mice (mouse nos. 4 and 6) observed by May-Grünwald Giemsa staining. Original magnification, ×400. (**H**) Pie chart illustrating the frequencies of the disease phenotypes of $Ezh2^{\Delta/\Delta}p53^{\Delta/\Delta}$ mice (n = 18). ETP-ALL with DN1, DN2, and DN1/2 type and thymic lymphoma were identified. (**I**) Representative flow cytometric profiles of CD4/CD8 expression in donor-derived $CD45.2^+$ cells, and c-Kit, CD44, and CD25 expression in $CD45.2^+Lin^-$ cells in the thymus of each subtype of ETP-ALL shown in **H**. (**J**) Representative histology of the thymus, spleen, and liver of an $Ezh2^{\Delta/\Delta}p53^{\Delta/\Delta}$ ETP-ALL mouse observed by H&E staining and CD3 staining. Original magnification, ×400 (left panels); ×100 (right panels). Scale bars: 100 μm. (**K**) Rearrangement of the TCR-β gene in DN2 cells from WT and $Ezh2^{\Delta/\Delta}p53^{\Delta/\Delta}$ mice 3 months after transplantation and ETP-ALL mice (mouse nos. 13 and 41) assessed by Dβ1-Jβ1 amplifications by PCR. Germline bands were observed in WT $Gr1^+Mac1^+$ neutrophils and $B220^+$ B cells.

(23). As expected, the enrichment of the gene signature of HSCs was significantly greater in $Ezh2^{\Delta/\Delta}p53^{\Delta/\Delta}$ ETP-ALL cells than in WT DN2 cells (Figure 5J), supporting the human ETP-ALL–like nature of $Ezh2^{\Delta/\Delta}p53^{\Delta/\Delta}$ leukemic cells. We confirmed that the expression of *Hlf* and *Hoxa10* was significantly stronger in $Ezh2^{\Delta/\Delta}p53^{\Delta/\Delta}$ ETP-ALL cells by quantitative PCR (Figure 5K). The JAK/STAT and Ras signaling pathways are generally activated in human ETP-ALL cells (2), and the loss of Ezh2 has been shown to enhance Stat3 phosphorylation in *p19*^{Arf}-deficient thymocytes (13). We also found that JAK/STAT and Ras signaling pathway genes were significantly activated in $Ezh2^{\Delta/\Delta}p53^{\Delta/\Delta}$ ETP-ALL cells (Supplemental Figure 5). The inactivation of PRC2 abrogated the transcriptional program of T cell development genes including *Runx1*, but resulted in the acquisition of some stem cell–associated gene signatures, leading to the enhanced proliferative capacity of leukemic cells in the absence of p53.

The loss of Ezh2 and p53 induces the propagation of DNA hypermethylation of critical T cell developmental regulators during the leukemic transformation. As described above, a significant portion of the canonical Ezh2-PRC2 targets were transcriptionally silenced or downregulated despite the absence of Ezh2, suggesting that an alternative mechanism is operating in this process during leukemic transformation. We previously reported that the loss of Ezh2 induced aberrant DNA hypermethylation in a significant portion of the CGIs of PRC2 targets in the $Lin^-Sca\text{-}1^+c\text{-}Kit^+$ (LSK) hematopoietic stem/progenitor cells of *Tet2* hypomorphic mice (*Tet2*$^{KD/KD}$), and found a critical role for this epigenetic switch in the pathogenesis of MDS that developed in $Ezh2^{\Delta/\Delta}Tet2^{KD/KD}$ mice (24). In order to elucidate whether this epigenetic switch also took place in $Ezh2^{\Delta/\Delta}p53^{\Delta/\Delta}$ ETP-ALL cells, we performed reduced representative bisulfite sequencing (RRBS) on DN2 cells isolated from WT, $Ezh2^{\Delta/\Delta}$, $p53^{\Delta/\Delta}$, and $Ezh2^{\Delta/\Delta}p53^{\Delta/\Delta}$ mice at the preleukemic stage and $Ezh2^{\Delta/\Delta}p53^{\Delta/\Delta}$ ETP-ALL DN2 cells. While neither $Ezh2^{\Delta/\Delta}$ cells nor $p53^{\Delta/\Delta}$ cells significantly gained hyperdifferentially methylated regions (hyper-DMRs) at the promoter regions (–2.5 kb to +0.5 kb from transcription start site [TSS]) compared with WT cells, DNA hypermethylation was mild in preleukemic $Ezh2^{\Delta/\Delta}p53^{\Delta/\Delta}$ cells and robust in $Ezh2^{\Delta/\Delta}p53^{\Delta/\Delta}$ leukemic cells (Figure 6A). Notably, $Ezh2^{\Delta/\Delta}p53^{\Delta/\Delta}$ leukemic cells established hyper-DMRs at a considerably larger portion of promoter regions than was seen in WT cells and exhibited only a few hypo-DMRs (Figure 6B). These results indicate that the deletion of *Ezh2* and *p53* alone was not sufficient to induce aberrant DNA hypermethylation, but induced aberrant DNA hypermethylation in a combinatorial manner, particularly during the development of leukemia. Gene ontology (GO) enrichment analyses revealed that hyper-DMRs in $Ezh2^{\Delta/\Delta}p53^{\Delta/\Delta}$ leukemic cells were significantly enriched in genes associated with development, cell adhesion, differentiation, and transcription factor activity (Figure 6C), while hypo-DMRs were enriched in a few categories, such as lipid catabolic processes (Figure 6C), suggesting that DNA hypermethylation plays a role in the development of ETP-ALL.

We then attempted to elucidate the relationship of epigenetic modifications between DNA methylation and H3K27me3 levels in $Ezh2^{\Delta/\Delta}p53^{\Delta/\Delta}$ leukemic cells at the promoter regions and found that hyper-DMRs were strongly associated with lower levels of H3K27me3 in $Ezh2^{\Delta/\Delta}p53^{\Delta/\Delta}$ leukemic cells than in WT cells (Figure 6D and Supplemental Figure 6). Furthermore, a significant portion (38%) of hyper-DMRs in $Ezh2^{\Delta/\Delta}p53^{\Delta/\Delta}$ leukemic cells were observed in the canonical PRC2 targets defined in WT DN1 cells (Supplemental Figure 7). Indeed, the PRC2 targets in WT DN1 cells acquired significantly higher levels of DNA methylation than all RefSeq genes in $Ezh2^{\Delta/\Delta}p53^{\Delta/\Delta}$ leukemic cells (Figure 6E). In contrast, the PRC2 targets did not gain DNA hypermethylation in $Ezh2^{\Delta/\Delta}$ cells, compared with WT cells (Figure 6E). These results indicate that the loss of both Ezh2 and p53 induce the epigenetic switch from H3K27me3 to DNA hypermethylation at the PRC2 target promoter regions during the development of leukemia.

DNA methylation levels at promoter regions do not necessarily correlate with gene expression levels (25, 26). Consistent with this finding, there was no correlation between the levels of DNA methylation and gene expression in $Ezh2^{\Delta/\Delta}$, $p53^{\Delta/\Delta}$, and $Ezh2^{\Delta/\Delta}p53^{\Delta/\Delta}$ DN2 cells and $Ezh2^{\Delta/\Delta}p53^{\Delta/\Delta}$ leukemic cells in the present study (Figure 6F and Supplemental Figure 8). However, we found an epigenetic switch from H3K27me3 to DNA methylation at the promoters of genes encoding nonhematopoietic developmental regulators (e.g., *Tbx1* and *Sox9*) as well as T cell development regulators (e.g., *Runx1* and *Nr4a3*) (Figure 6G) associated with reduced levels of expression in $Ezh2^{\Delta/\Delta}p53^{\Delta/\Delta}$ leukemic cells (Figure 5, D and F). These results imply that the epigenetic switch reinforced the transcriptional repression of key T cell regulator genes, thereby promoting the pathogenesis of ETP-ALL.

Aberrant DNA hypermethylation contributes to the pathogenesis of ETP-ALL. In order to understand the molecular

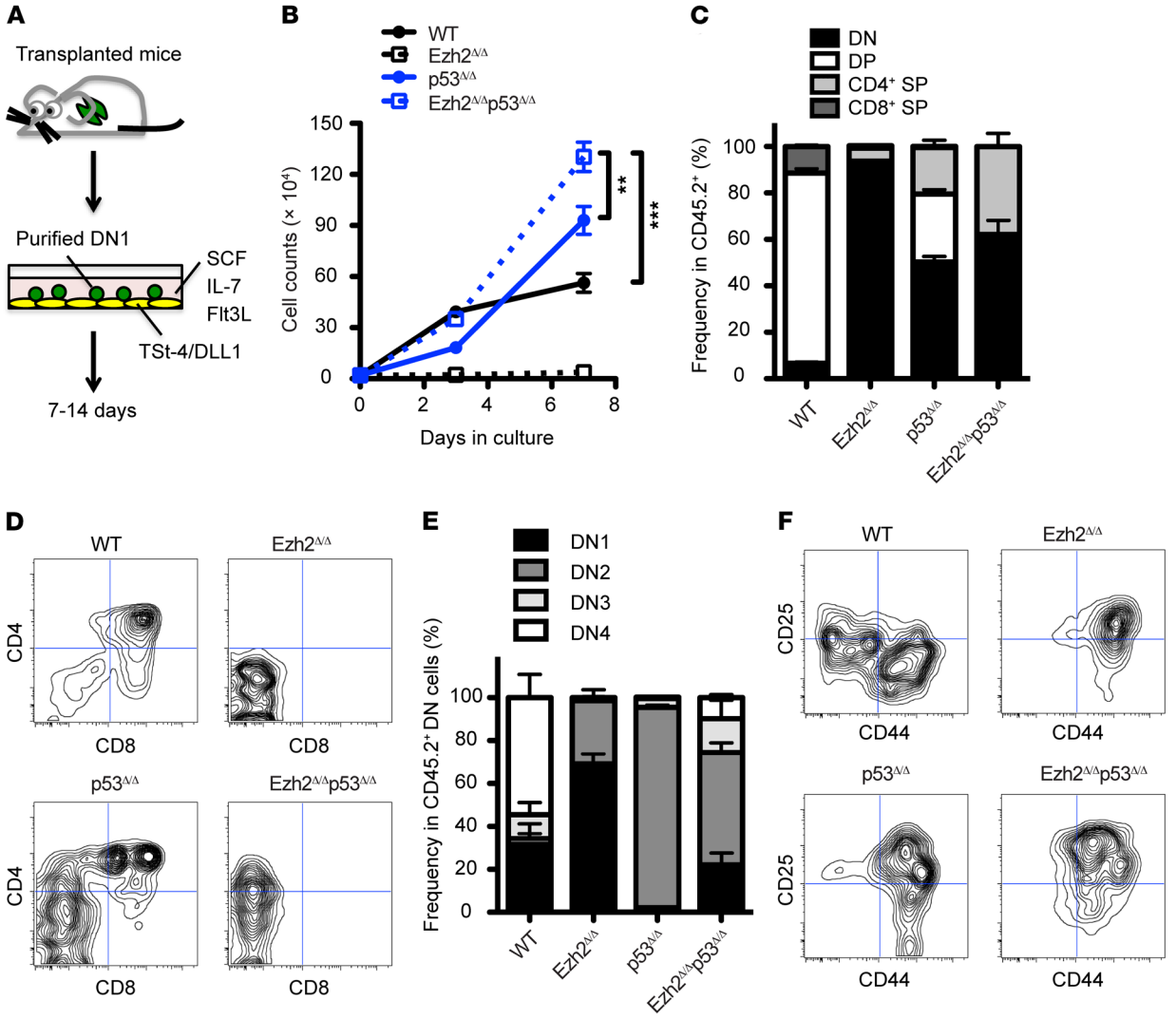

Figure 3. The loss of Ezh2 impeded T cell differentiation at the CD4⁻CD8⁻ stage. (**A**) Experimental schematic of the procedure to examine the T cell differentiation potential of purified CD45.2⁺CD44⁺CD25⁻Lin⁻ DN1 cells. DN1 cells were cultured with TSt-4/DLL1 stromal cells in the presence of SCF, IL-7, and Flt3L (10 ng/ml) for 7 to 14 days. (**B**) Total cell counts of WT (black line), Ezh2$^{\Delta/\Delta}$ (black broken line), p53$^{\Delta/\Delta}$ (blue line), and Ezh2$^{\Delta/\Delta}$p53$^{\Delta/\Delta}$ (broken blue line) cells during culture (n = 3–6). Data are shown as mean ± SEM. $^{**}P < 0.01$; $^{***}P < 0.001$, Student's t test. (**C**) Proportions of CD4⁺CD8⁺ cells in CD45.2⁺ cells on day 7 of WT, Ezh2$^{\Delta/\Delta}$, p53$^{\Delta/\Delta}$, and Ezh2$^{\Delta/\Delta}$p53$^{\Delta/\Delta}$ DN1 cell culture (n = 3–6). Data are shown as mean ± SEM. (**D**) Representative flow cytometric profiles of CD4 and CD8 expression in WT, Ezh2$^{\Delta/\Delta}$, p53$^{\Delta/\Delta}$, and Ezh2$^{\Delta/\Delta}$p53$^{\Delta/\Delta}$ CD45.2⁺ cells on day 7 of the culture. (**E**) Proportions of DN1, DN2, DN3, and DN4 cells in CD45.2⁺CD4⁻CD8⁻ DN cells on day 7 of the culture (n = 3–6). Data are shown as mean ± SEM. (**F**) Representative flow cytometric profiles of CD44 and CD25 expression in CD45.2⁺CD4⁻CD8⁻ cells on day 7 of the culture. Data are representative of 2 independent experiments.

mechanisms underlying the epigenetic switch, we examined expression of *Dnmt1*, *Dnmt3a*, and *Dnmt3b* in DN2 cells by quantitative PCR and found that Ezh2$^{\Delta/\Delta}$p53$^{\Delta/\Delta}$ leukemic cells expressed *Dnmt* genes at levels similar to those of DN2 cells with other genotypes and Ezh2$^{\Delta/\Delta}$p53$^{\Delta/\Delta}$ cells at the preleukemic stage (Supplemental Figure 9). We next asked whether pathogenic DNA hypermethylation in these key genes contributed to leukemic transformation. We first knocked down *Dnmt1*, *Dnmt3a*, or *Dnmt3b* by utilizing individual shRNA vectors (Supplemental Figure 10) and assessed the impact of knocking down these methyltransferases in EPT-ALL DN1/2 cells. We found that knockdown of individual *Dnmt* genes was not effective in canceling the differentiation block of ETP-ALL cells and only partially promoted the differentiation of ETP-ALL cells beyond the DN3 stage, but hardly into DP cells (Supplemental Figure 11), implying that *Dnmt1*, *Dnmt3a*, and *Dnmt3b* establish aberrant DNA hypermethylation and induce the differentiation block in a combinatorial manner.

We then assessed the efficacy of the DNA hypomethylating agent DAC at canceling the differentiation block of Ezh2$^{\Delta/\Delta}$p53$^{\Delta/\Delta}$ leukemic cells. Under in vitro differentiation conditions, the DAC treatment did not affect the growth or differentiation of WT DN1/2 cells (data not shown). In contrast, DAC markedly suppressed the growth of Ezh2$^{\Delta/\Delta}$p53$^{\Delta/\Delta}$ CD44⁺CD25^{mid} leukemic cells in a dose-dependent manner (Figure 7A) and successfully induced the differentiation of leukemic cells into the DP and CD8⁺ SP stages (Figure 7, B and C). The recovery of the expression of *Nr4a3* and *Bcl11b* was significantly greater, while the expression of *Runx1* was moderately

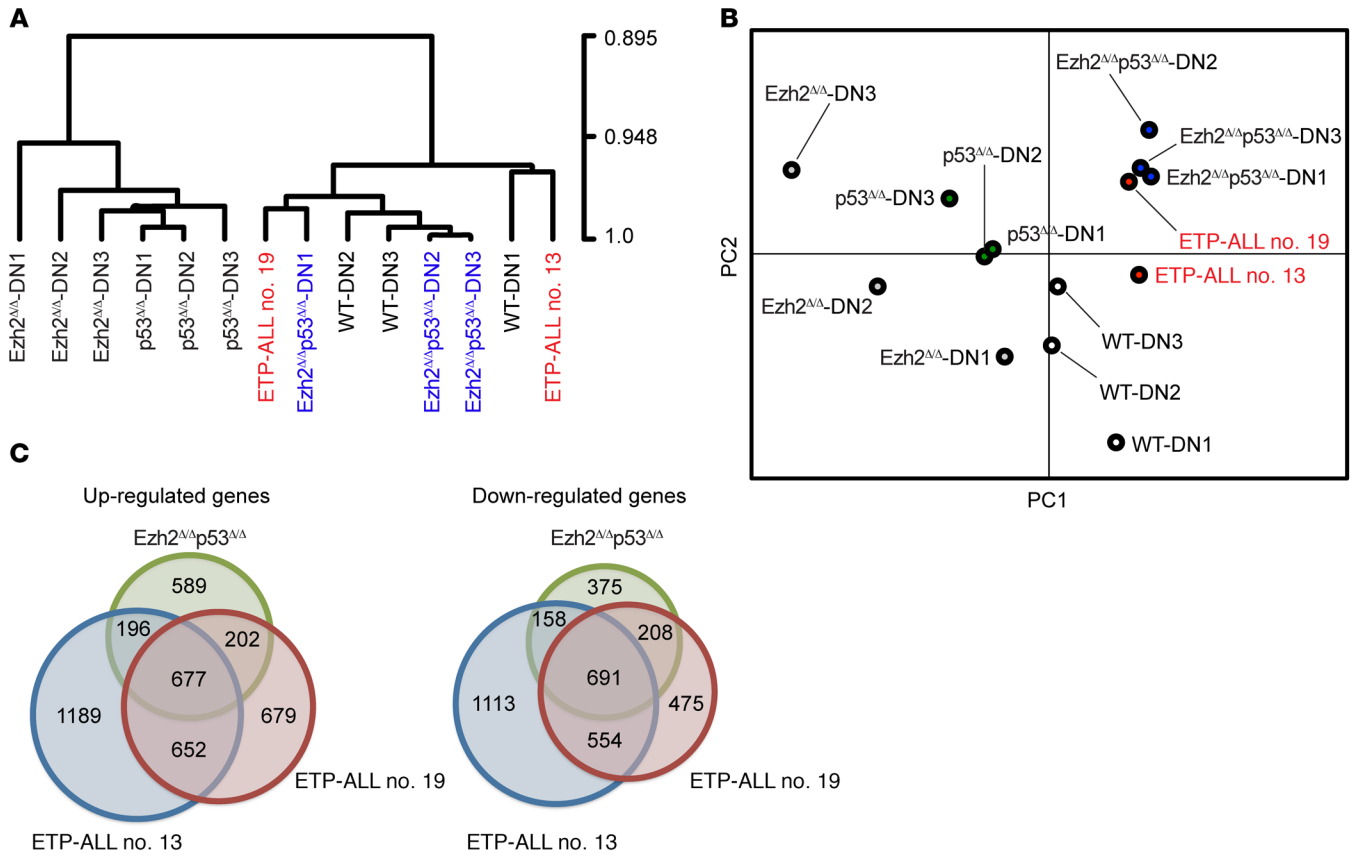

Figure 4. Concurrent loss of Ezh2 and p53 impaired the transcriptional program of T cell differentiation. (**A**) Hierarchical clustering based on total gene expression in DN1, DN2, and DN3 cells isolated from WT, $Ezh2^{\Delta/\Delta}$, $p53^{\Delta/\Delta}$, and $Ezh2^{\Delta/\Delta}p53^{\Delta/\Delta}$ mice 3 months after transplantation (n = 5–10) and in DN2 leukemic cells isolated from 2 distinct $Ezh2^{\Delta/\Delta}p53^{\Delta/\Delta}$ ETP-ALL mice (mouse nos. 13 and 19). Linkage scores are indicated on the right. (**B**) A principal component (PC) analysis based on total gene expression in DN1, DN2, and DN3 cells isolated from WT mice (white circles), $Ezh2^{\Delta/\Delta}$ mice (gray circles), $p53^{\Delta/\Delta}$ mice (green circles), $Ezh2^{\Delta/\Delta}p53^{\Delta/\Delta}$ mice at a predisease stage (blue circles), and DN2 leukemic cells from $Ezh2^{\Delta/\Delta}p53^{\Delta/\Delta}$ ETP-ALL mice (red circles). (**C**) Venn diagrams showing overlaps of upregulated and downregulated genes (left and right panels, respectively) between DN2 cells from $Ezh2^{\Delta/\Delta}p53^{\Delta/\Delta}$ mice 3 months after transplantation and $Ezh2^{\Delta/\Delta}p53^{\Delta/\Delta}$ ETP-ALL mice (nos. 13 and 19), relative to gene expression in WT DN2 cells.

stronger in DAC-treated leukemic cells than in dimethylsulfoxide–treated (DMSO-treated) leukemic cells (Figure 7D), indicating that the restored expression of T cell development regulators coordinated to enforce the terminal differentiation of ETP leukemic cells.

In order to examine the impact of DAC on pathogenic DNA hypermethylation in $Ezh2^{\Delta/\Delta}p53^{\Delta/\Delta}$ leukemic cells, we performed RRBS on DMSO-treated DN2 leukemic cells and DAC-induced DN4 cells in the culture. We found that DNA methylation levels at CGIs and promoter regions were significantly lower in DAC-induced DN4 cells than in control DN2 cells (Figure 7E), as represented at the *Nr4a3* locus (Figure 7F). In addition, GO analysis revealed that hypo-DMRs in DAC-induced DN4 cells compared with control DN2 cells were significantly enriched in genes with development, cell adhesion, differentiation, and transcription factor activity (Figure 7G). These results indicate that pathogenic DNA hypermethylation in key regulatory genes abrogated the operation of the normal network of T cell development genes and contributed to the pathogenesis of ETP-ALL.

Finally, in order to examine whether DAC inhibits the development of ETP-ALL in vivo, we transplanted $Ezh2^{\Delta/\Delta}$ $p53^{\Delta/\Delta}$ ETP-ALL cells (1×10^6 cells) together with 2×10^6 WT BM cells into lethally irradiated recipient mice and treated the recipient mice with DAC (0.2 mg/kg) or DMSO from 3 weeks after transplantation. Although DAC did not release the differentiation block of leukemic cells in this setting (data not shown), we observed that DAC impeded the expansion of leukemic cells, as evident in the reduced proportion of leukemic cells in the PB (Figure 7H). Consequently, DAC treatment extended the survival of recipient mice (Figure 7I), although the statistical significance was marginal, supporting the idea that DAC would be warranted for a therapy on patients with ETP-ALL harboring the EZH2 mutation.

Discussion

ETP-ALL is a new disease entity of T cell malignancies with a poor clinical outcome. ETP-ALL cells harbor high frequencies of deletions and/or loss-of-function mutations in PRC2, including *EZH2*. *EZH2* has been characterized as an oncogene in many cancers, including B cell lymphoma, in which gain-of-function mutations in EZH2 play a pathogenic role (27, 28), and acute myeloid leukemia (AML) (29, 30). Recently, gain-of-function mutations in *EZH2* have been shown to be neomorphic because $Ezh2^{Y641F}$ globally increased the levels of H3K27me3, but also induced loss of H3K27me3 modification in a region-dependent manner that

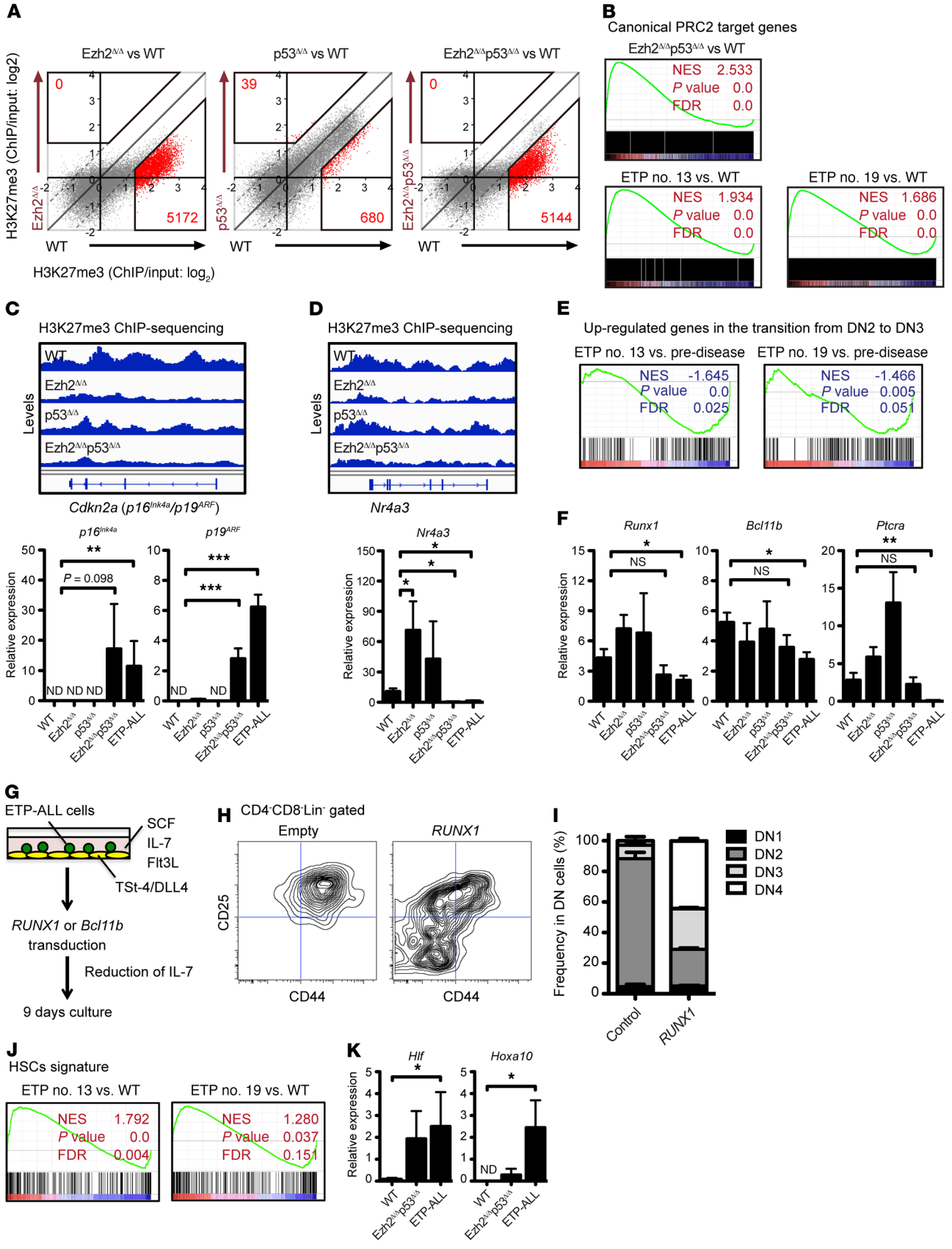
A
Ezh2Δ/Δ vs WT
p53Δ/Δ vs WT
Ezh2Δ/Δp53Δ/Δ vs WT
H3K27me3 (ChIP/input: log2)
0
39
0
5172
680
5144
WT
H3K27me3 (ChIP/input: log2)
B
Canonical PRC2 target genes
Ezh2Δ/Δp53Δ/Δ vs WT
NES 2.533
P value 0.0
FDR 0.0
ETP no. 13 vs. WT
NES 1.934
P value 0.0
FDR 0.0
ETP no. 19 vs. WT
NES 1.686
P value 0.0
FDR 0.0
C
H3K27me3 ChIP-sequencing
WT
Ezh2Δ/Δ
p53Δ/Δ
Ezh2Δ/Δp53Δ/Δ
Levels
Cdkn2a (p16Ink4a/p19ARF)
p16Ink4a
p19ARF
P = 0.098
ND ND ND
ND
ND
Relative expression
WT
Ezh2Δ/Δ
p53Δ/Δ
Ezh2Δ/Δp53Δ/Δ
ETP-ALL
D
H3K27me3 ChIP-sequencing
Nr4a3
E
Up-regulated genes in the transition from DN2 to DN3
ETP no. 13 vs. pre-disease
NES -1.645
P value 0.0
FDR 0.025
ETP no. 19 vs. pre-disease
NES -1.466
P value 0.005
FDR 0.051
F
Runx1
Bcl11b
Ptcra
NS
G
ETP-ALL cells
SCF
IL-7
Flt3L
TSt-4/DLL4
RUNX1 or Bcl11b
transduction
Reduction of IL-7
9 days culture
H
CD4-CD8-Lin- gated
Empty
RUNX1
CD25
CD44
I
Frequency in DN cells (%)
DN1
DN2
DN3
DN4
Control
RUNX1
J
HSCs signature
ETP no. 13 vs. WT
NES 1.792
P value 0.0
FDR 0.004
ETP no. 19 vs. WT
NES 1.280
P value 0.037
FDR 0.151
K
Hlf
Hoxa10
ND

Figure 5. Ezh2 loss led to the silencing of critical T cell lineage determinants. (**A**) Scatter plots showing the relationship of the fold enrichment values (ChIP/input) of H3K27me3 (TSS ±2.0 kb of RefSeq genes) between WT, Ezh2$^{\Delta/\Delta}$, p53$^{\Delta/\Delta}$, and Ezh2$^{\Delta/\Delta}$p53$^{\Delta/\Delta}$ DN1 (CD44$^+$CD25$^-$Lin$^-$) cells 2 months after the deletion of *Ezh2* and/or *p53*. (**B**) GSEA plots for canonical PRC2 target genes comparing DN2 cells from WT mice to DN2 cells from Ezh2$^{\Delta/\Delta}$ p53$^{\Delta/\Delta}$ mice at a predisease stage and 2 distinct Ezh2$^{\Delta/\Delta}$p53$^{\Delta/\Delta}$ ETP-ALL mice (nos. 13 and 19). Normalized enrichment score (NES), nominal *P* value, and FDR *q* values are indicated. (**C**) ChIP-seq view of H3K27me3 levels at the *Cdkn2a* locus in WT, Ezh2$^{\Delta/\Delta}$, p53$^{\Delta/\Delta}$, and Ezh2$^{\Delta/\Delta}$p53$^{\Delta/\Delta}$ DN1 cells (top), and a quantitative RT-PCR analysis of the expression of *p16^{Ink4a}* and *p19^{Arf}* in DN2 cells isolated from WT (*n* = 12), Ezh2$^{\Delta/\Delta}$ (*n* = 6), p53$^{\Delta/\Delta}$ (*n* = 6), and Ezh2$^{\Delta/\Delta}$ p53$^{\Delta/\Delta}$ (*n* = 8) mice 3 months after transplantation and ETP-ALL mice (*n* = 8) (bottom). (**D**) ChIP-seq view of H3K27me3 levels at the *Nr4a3* locus in WT, Ezh2$^{\Delta/\Delta}$, p53$^{\Delta/\Delta}$, and Ezh2$^{\Delta/\Delta}$p53$^{\Delta/\Delta}$ DN1 cells (top), and quantitative RT-PCR data of the expression of *Nr4a3* in DN2 cells isolated from WT (*n* = 12), Ezh2$^{\Delta/\Delta}$ (*n* = 6), p53$^{\Delta/\Delta}$ (*n* = 6), and Ezh2$^{\Delta/\Delta}$p53$^{\Delta/\Delta}$ (*n* = 8) mice 3 months after transplantation and ETP-ALL mice (*n* = 8) (bottom) $^*P < 0.001$. (**E**) GSEA plots for T cell differentiation regulators, which were upregulated at the transition from DN2 to DN3 stages (19), comparing the DN2 cells of 2 distinct Ezh2$^{\Delta/\Delta}$p53$^{\Delta/\Delta}$ ETP-ALL mice (nos. 13 and 19) with those of Ezh2$^{\Delta/\Delta}$p53$^{\Delta/\Delta}$ mice 3 months after transplantation. (**F**) Quantitative RT-PCR analysis of the expression of *Runx1*, *Bcl11b*, and *Ptcra* in DN2 cells isolated from WT (*n* = 12), Ezh2$^{\Delta/\Delta}$ (*n* = 6), p53$^{\Delta/\Delta}$ (*n* = 6), and Ezh2$^{\Delta/\Delta}$p53$^{\Delta/\Delta}$ (*n* = 8) mice 3 months after transplantation and Ezh2$^{\Delta/\Delta}$p53$^{\Delta/\Delta}$ ETP-ALL mice (*n* = 8). (**G**) Experimental schematic of the procedure to examine the T cell differentiation of Ezh2$^{\Delta/\Delta}$p53$^{\Delta/\Delta}$ leukemic cells. (**H**) Representative flow cytometric profiles of CD44 and CD25 expression in CD4$^-$CD8$^-$Lin$^-$GFP$^+$ transduced leukemic cells on day 9 of the culture (*n* = 3). Data are representative of 2 independent experiments. (**I**) Proportions of DN1, DN2, DN3, and DN4 cells in CD4$^-$CD8$^-$Lin$^-$GFP$^+$ transduced leukemic cells on day 9 of the control and *RUNX1* cultures (*n* = 3). (**J**) GSEA plots for the gene expression signatures of HSCs comparing DN2 cells isolated from WT mice and 2 distinct Ezh2$^{\Delta/\Delta}$p53$^{\Delta/\Delta}$ ETP-ALL mice. (**K**) Quantitative RT-PCR analysis of the expression of *Hlf* and *Hoxa10* in DN2 cells isolated from WT (*n* = 12) and Ezh2$^{\Delta/\Delta}$p53$^{\Delta/\Delta}$ (*n* = 8) mice 3 months after transplantation and Ezh2$^{\Delta/\Delta}$p53$^{\Delta/\Delta}$ ETP-ALL mice (*n* = 8). (**C**, **D**, **F**, and **K**) Data are shown as mean ± SEM. $^*P < 0.05$; $^{**}P < 0.01$; $^{***}P < 0.001$, Student's *t* test (**F** [*Runx1*, *Bcl11b*]); Mann-Whitney *U* test (**C**, **D**, **K**, **F** [*Ptcra*]).

was associated with increased transcription of target genes (31). In contrast, EZH2-PRC2 functions as a tumor suppressor in MDS as well as T cell malignancies. We previously demonstrated how the hematopoietic cell–specific deletion of *Ezh2* promoted the development of MDS and/or MPN diseases in concert with the loss of *Tet2*, *RUNX1* mutants, or the *JAK2^{V671F}* mutant (8–10). We and others also previously reported that *Ezh2*-deficient mice showed impaired T cell production due to perturbed differentiation at the DN cell stage (3, 32). We subsequently reported that the serial transplantation of *Ezh2*-deficient BM cells induced CD8$^+$ T-ALL, but not ETP-ALL, despite its low frequency (11). In the present study, we demonstrated that the loss of *Ezh2* and *p53* collaborated to initiate monoclonal CD4$^{-/mid}$CD8$^-$c-Kit$^+$CD44$^+$ ETP-like leukemia in mice, which recapitulated ETP-ALL in patients. These results indicate that Ezh2 functions to ensure T cell development at multiple differentiation stages from BM HSCs to mature T cells and that its inactivation promotes ETP and non-ETP T-ALL in a context-dependent manner.

Early T cell development depends on the proliferation and differentiation of multipotent progenitor cells that undergo T cell commitment and TCR rearrangement at the CD4$^-$CD8$^-$ DN stage. These processes are initiated by Notch signaling in the thymus and are sequentially operated by networks of differentiation regulator genes. To this end, transcriptional and epigenetic machineries function to promote T cell commitment and silence the expression of stem and progenitor cell genes, resulting in the loss of other lineage potentials, including myeloid cells (33). Transcription factor networks, including *Bcl11b*, are required for T cell commitment and the loss of myeloid cell potential at the DN2b stage (20, 21). In the present study, we demonstrated that *Ezh2p53*-deficient leukemic cells suppressed the expression of pivotal genes for T cell development, such as *Runx1* and *Bcl11b*, but sustained the expression of stem cell signature genes, which are associated with the self-renewal capacity of normal c-Kit$^+$ ETP cells. In the *NRas^{Q61K}Cdkn2a$^{-/-}$* ETP-ALL mouse model previously reported, stem and myeloid progenitor signature genes, including *Hoxa9*, were aberrantly expressed in *Ezh2*-deficient leukemic cells because Ezh2-PRC2 directly suppresses *Hoxa9* in this setting. The forced expression of *Hoxa9* promoted the proliferation of *NRas^{Q61K}Cdkn2a$^{-/-}$* ETP-ALL cells (13) and also the transformation of *Ezh2*-deficient MDS to AML (9). However, *Ezh2p53*-deficient ETP leukemic cells did not show the increased expression of *Hoxa9* or reduced levels of H3K27me3 at the promoter region of *Hoxa9* (data not shown). This discrepancy may be due to the different experimental strategies used to induce ETP-ALL–like cells in vitro versus in vivo. Nevertheless, the expression of stem and myeloid progenitor signature genes was enhanced in both ETP-ALL mouse models. Further studies are needed in order to elucidate how the inappropriate expression of these genes promotes the transformation of ETPs.

We recently showed that an epigenetic switch from H3K27me3 to DNA methylation occurs following the loss of Ezh2 in Tet2$^{KD/KD}$ mice and maintains the transcriptional repression of a significant portion of PRC2 targets, thereby contributing to the progression of MDS (24). We found that this epigenetic switch was accentuated at the promoter regions of pivotal transcriptional regulator genes in *Ezh2p53*-deficient ETP-ALL cells, the silencing of which impedes the proper ensemble of transcription factors for T cell development. Correspondingly, neither *RUNX1* nor *Bcl11b* transduction alone induced the differentiation of ETP-ALL cells into mature CD4$^+$CD8$^+$ cells in vitro; however, DAC treatment resulted in the terminal differentiation of ETP-ALL cells following the reactivation of a set of genes encoding transcriptional regulators of T cell development. These results indicate that the DNA methylation–mediated inhibition of the gene networks of T cell development, rather than that of a single transcription factor, was largely responsible for the differentiation block of ETPs and aberrant expression of stem/myeloid genes during the development of ETP-ALL. A functional link between DNA methylation and PRC2 has been implicated in the regulation of the biological processes of development, differentiation, and cancer (34, 35). Previous studies showed that DNA hypermethylation in cancer, including leukemia, correlated with bivalent genes marked by trithorax group–mediated H3K4me3 and PRC2-mediated H3K27me3, which are activated upon the differentiation of ES cells (36, 37). As we previously reported in *Ezh2*-deficient MDS cells (24), *Ezh2p53*-deficient ETP-ALL cells acquired higher levels of DNA methylation at the CGI promoter regions of PRC2 target genes. Of interest, Fbxl10/Kdm2b, a component of noncanonical PRC1, has been shown to protect the CGI promoters of polycomb-bound genes from DNA

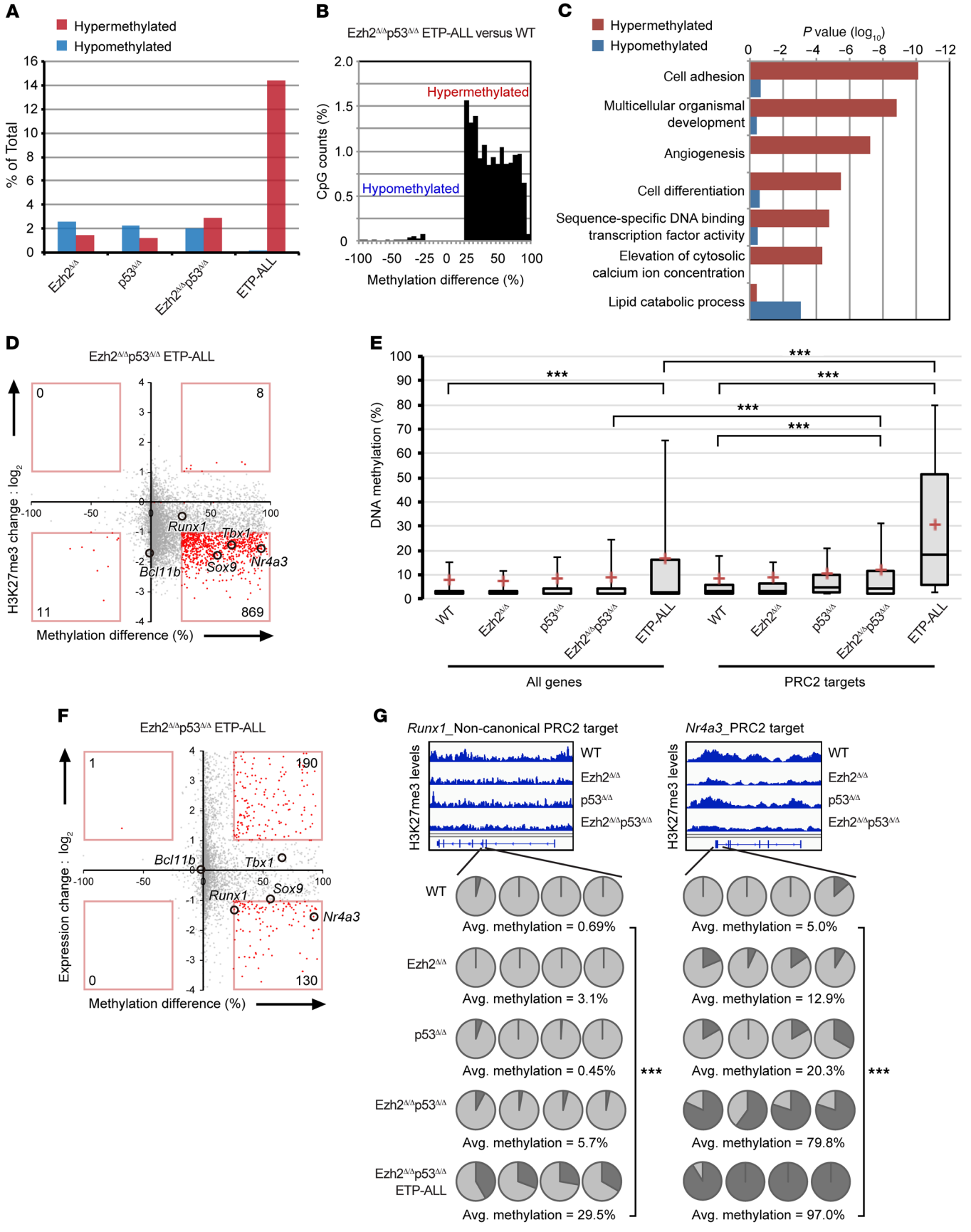
A
Hypermethylated
Hypomethylated
% of Total
Ezh2Δ/Δ
p53Δ/Δ
Ezh2Δ/Δp53Δ/Δ
ETP-ALL
B
Ezh2Δ/Δp53Δ/Δ ETP-ALL versus WT
Hypermethylated
Hypomethylated
CpG counts (%)
Methylation difference (%)
C
Hypermethylated
Hypomethylated
P value (log10)
Cell adhesion
Multicellular organismal development
Angiogenesis
Cell differentiation
Sequence-specific DNA binding transcription factor activity
Elevation of cytosolic calcium ion concentration
Lipid catabolic process
D
Ezh2Δ/Δp53Δ/Δ ETP-ALL
H3K27me3 change : log2
Methylation difference (%)
Runx1
Tbx1
Bcl11b
Sox9
Nr4a3
E
DNA methylation (%)
All genes
PRC2 targets
F
Ezh2Δ/Δp53Δ/Δ ETP-ALL
Expression change : log2
Methylation difference (%)
G
Runx1_Non-canonical PRC2 target
Nr4a3_PRC2 target
H3K27me3 levels
WT
Ezh2Δ/Δ
p53Δ/Δ
Ezh2Δ/Δp53Δ/Δ
Avg. methylation = 0.69%
Avg. methylation = 5.0%
Avg. methylation = 3.1%
Avg. methylation = 12.9%
Avg. methylation = 0.45%
Avg. methylation = 20.3%
Avg. methylation = 5.7%
Avg. methylation = 79.8%
Avg. methylation = 29.5%
Avg. methylation = 97.0%
ETP-ALL

Figure 6. DNA hypermethylation propagated at promoters of critical genes for T cell developmental regulators following the loss of Ezh2 and p53. (**A**) Numbers of hypo- and hyper-DMRs at promoters in Ezh2$^{\Delta/\Delta}$ DN2 cells, p53$^{\Delta/\Delta}$ DN2 cells, Ezh2$^{\Delta/\Delta}$p53$^{\Delta/\Delta}$ DN2 cells at the preleukemic stage, and Ezh2$^{\Delta/\Delta}$p53$^{\Delta/\Delta}$ leukemic DN2 cells relative to WT DN2 cells. (**B**) Bars showing differences in the degree of methylation (%) between Ezh2$^{\Delta/\Delta}$ p53$^{\Delta/\Delta}$ leukemic DN2 cells and WT DN2 cells. (**C**) GO biological process gene sets significantly enriched in hyper-DMR (red bars) and hypo-DMR (blue bars) genes in Ezh2$^{\Delta/\Delta}$p53$^{\Delta/\Delta}$ leukemic cells. (**D**) Scatter plots showing the relationship between the fold enrichment values (ChIP/input) of H3K27me3 (TSS ± 2.0 kb of RefSeq genes) in Ezh2$^{\Delta/\Delta}$p53$^{\Delta/\Delta}$ leukemic DN1 cells relative to WT DN1 cells and methylation differences in Ezh2$^{\Delta/\Delta}$p53$^{\Delta/\Delta}$ leukemic DN2 cells relative to WT DN2 cells. (**E**) Boxes showing the levels of DNA methylation (%) of WT DN2 cells, Ezh2$^{\Delta/\Delta}$ DN2 cells, p53$^{\Delta/\Delta}$ DN2 cells, and Ezh2$^{\Delta/\Delta}$p53$^{\Delta/\Delta}$ DN2 cells at the preleukemic stage and Ezh2$^{\Delta/\Delta}$ p53$^{\Delta/\Delta}$ leukemic DN2 cells in RefSeq genes (All genes) and canonical PRC2 target genes (PRC2 targets). Data are shown as box-and-whiskers plots drawing 10th to 90th percentiles. ***$P < 0.001$, Student's *t* test. (**F**) Scatter plots showing the relationship between expression changes in RefSeq genes in Ezh2$^{\Delta/\Delta}$p53$^{\Delta/\Delta}$ leukemic DN2 cells from those in WT DN2 cells and methylation differences in Ezh2$^{\Delta/\Delta}$p53$^{\Delta/\Delta}$ leukemic DN2 cells from those in WT DN2 cells. (**G**) ChIP-seq views of H3K27me3 and RRBS data of selected hyper-DMRs in WT DN2 cells, Ezh2$^{\Delta/\Delta}$ DN2 cells, p53$^{\Delta/\Delta}$ DN2 cells, and Ezh2$^{\Delta/\Delta}$p53$^{\Delta/\Delta}$ DN2 cells at the preleukemic stage and Ezh2$^{\Delta/\Delta}$p53$^{\Delta/\Delta}$ leukemic DN2 cells. Methylation differences between Ezh2$^{\Delta/\Delta}$p53$^{\Delta/\Delta}$ leukemic DN2 and WT DN2 cells that were significant are indicated. ***$P < 0.001$, Student's *t* test.

methylation (38). Taken together, these findings show that Ezh2-PRC2 may function to protect DNA methylation–prone CGI promoters from inappropriate DNA methylation in ETPs; however, once Ezh2-PCR2 is lost, the pathogenic epigenetic switch occurs at the gene loci of T cell development regulator genes, including tumor suppressor genes, such as *Runx1*, and promotes the transformation of ETPs.

While the loss of Ezh2-activated stem cell signature genes may confer an enhanced proliferative capacity to ETP-ALL cells, we also noted that RAS and JAK/STAT signaling pathways were both markedly activated in *Ezh2p53*-deficient leukemic cells from gene expression analyses. Patients with ETP-ALL frequently harbor activating mutations in genes involved in cytokine receptor and RAS signaling, such as *IL7R*, *JAK1*, *NRAS*, and *KRAS* (2). Gain-of function mutations in *IL7R* lead to the ligand-independent activation of JAK1/STAT5 signaling (39), and the transduction of the *IL7R* mutant in purified *p19^{Arf}*-deficient thymocytes was sufficient to generate an ETP-ALL–like disease in mice (40). As described above, another mouse model utilizing the *NRAS* mutant and purified *p19^{Arf}*-deficient thymocytes also showed enhanced Stat3 phosphorylation upon the loss of Ezh2. Consistent with these findings, we found that a cytokine stimulation activated the JAK/STAT signal more strongly in *Ezh2*-deficient hematopoietic stem/progenitor cells than in WT cells (10). Human ETP-ALL cells show higher phosphorylation levels of STAT5 and STAT3 in response to an IL-7 stimulation than non-ETP T-ALL cells (41). In fact, the pharmacological inhibition of JAK/STAT signaling by the JAK2 inhibitor ruxolitinib resulted in significant antitumor effects in mice and xenograft models (40, 41). Although the mechanisms by which the inactivation of EZH2-PRC2 stimulates JAK/STAT signaling currently remain unknown, our mouse model also supports the importance of JAK/STAT signaling for the pathogenesis of ETP-ALL regardless of the presence of JAK/STAT pathway mutations, raising the therapeutic potential of the combination of ruxolitinib and DAC in ETP-ALL patients harboring PRC2 mutations. *NOTCH1*-activating mutations were not frequently detected in ETP-ALL cells in patients or mice (2, 40). Correspondingly, the significant activation of Notch1 target genes was not observed in *Ezh2p53*-deficient ETP-ALL cells in the present study (data not shown).

Collectively, we demonstrated that the combined deletion of *Ezh2* and *p53* in mice successfully recapitulated ETP-ALL, a subset of T-ALL showing poor clinical outcomes, for which novel therapies are needed. The loss of Ezh2 in ETPs induced the pathogenic epigenetic switch from H3K27me3 to DNA methylation of pivotal T cell development regulators, such as *Runx1*, and promoted the transformation of ETPs. Our results strongly support a pathogenic role for inactivating PRC2 mutations in ETP-ALL, thereby highlighting a tumor-suppressive function for EZH2-PRC2 in ETPs.

Methods

Mice and transplantation. *Ezh2* conditional knockout (*Ezh2$^{fl/fl}$*) mice were described previously (42). These were crossed with *Rosa26::Cre-ERT2* mice (TaconicArtemis GmbH) for conditional deletion. *p53* conditional knockout (*p53$^{fl/fl}$*) mice were described previously (17). C57BL/6 mice congenic for the Ly5 locus (CD45.1) were purchased from Sankyo-Lab Service. A total of 5×10^6 BM cells were intravenously injected into 8.5 Gy– or 9 Gy–irradiated CD45.1$^+$ mice. Four weeks after transplantation, 1 mg tamoxifen (T5648, Sigma-Aldrich) was administered via an intraperitoneal injection for 5 consecutive days to completely delete the *p53* and *Ezh2* alleles.

Plasmids and retroviral transduction. Retroviral transduction of *pMYs-IRES-GFP*, *pMYs-RUNX1-IRES-GFP*, and *pMYs-Bcl11b-IRES-GFP* vectors into thymocytes was previously described (9, 43). Briefly, ETP-ALL cells were transduced with a vector on TSt-4/DLL1 stromal cells in the presence of SCF, IL-7, and Flt3L (10 ng/ml). In order to induce differentiation, transduced cells were cultured in the presence of SCF, IL-7, and Flt3L (2 ng/ml) for 9 days. For knockdown of *Dnmt*, *CS-H1-shRNA-EF-1α-EGFP* vector expressing shRNA-directed *Dnmt1*, *Dnmt3a*, *Dnmt3b*, or *Luciferase* was used. Target sequences were as follows: sh*Dnmt1* no. 1: ATCTATGGAAGGTGGTATTA; sh*Dnmt1* no.2: TATATGAAGACCTGATCAAT; sh*Dnmt3a* no.1: GCACAACAGAGAAACCTAA; sh*Dnmt3a* no.2: GCAGACCAACATCGAATCCAT; sh *Dnmt3b* no.1: GCGGGTATGAGGAGTGCATTA; and sh*Dnmt3b* no.2: CCAAGCGCCTCAAGACAAAT.

Flow cytometry and antibodies. Flow cytometry and cell sorting were performed by utilizing the following monoclonal antibodies: CD45.2 (clone 104), CD45.1 (clone A20), Gr1 (clone RB6-8C5), CD11b/Mac1 (clone M1/70), CD11c (clone N418), NK1.1 (clone PK136), Ter119 (catalog 116204), CD71 (clone R17217), CD127/IL-7Rα (clone A7R34), B220 (clone RA3-6B2), CD3e (clone 145-2C11), CD4 (clone L3T4), CD8α (clone 53-6.7), CD117/c-Kit (clone 2B8), Sca1 (clone D7), CD34 (clone MEC14.7), and FcγRII-III (clone 93). The CD34 antibody was purchased from eBioscience. All others were from BioLegend. The lineage mixture solution contained biotin-conjugated anti-Gr1, anti-Mac1, anti-CD11c, anti-NK1.1, anti-B220, anti-CD3e, anti-CD4, anti-CD8α, and anti-Ter119 antibodies. All flow cytometry analyses and cell sorting were performed on FACSAriaII or FACSCantoII (BD).

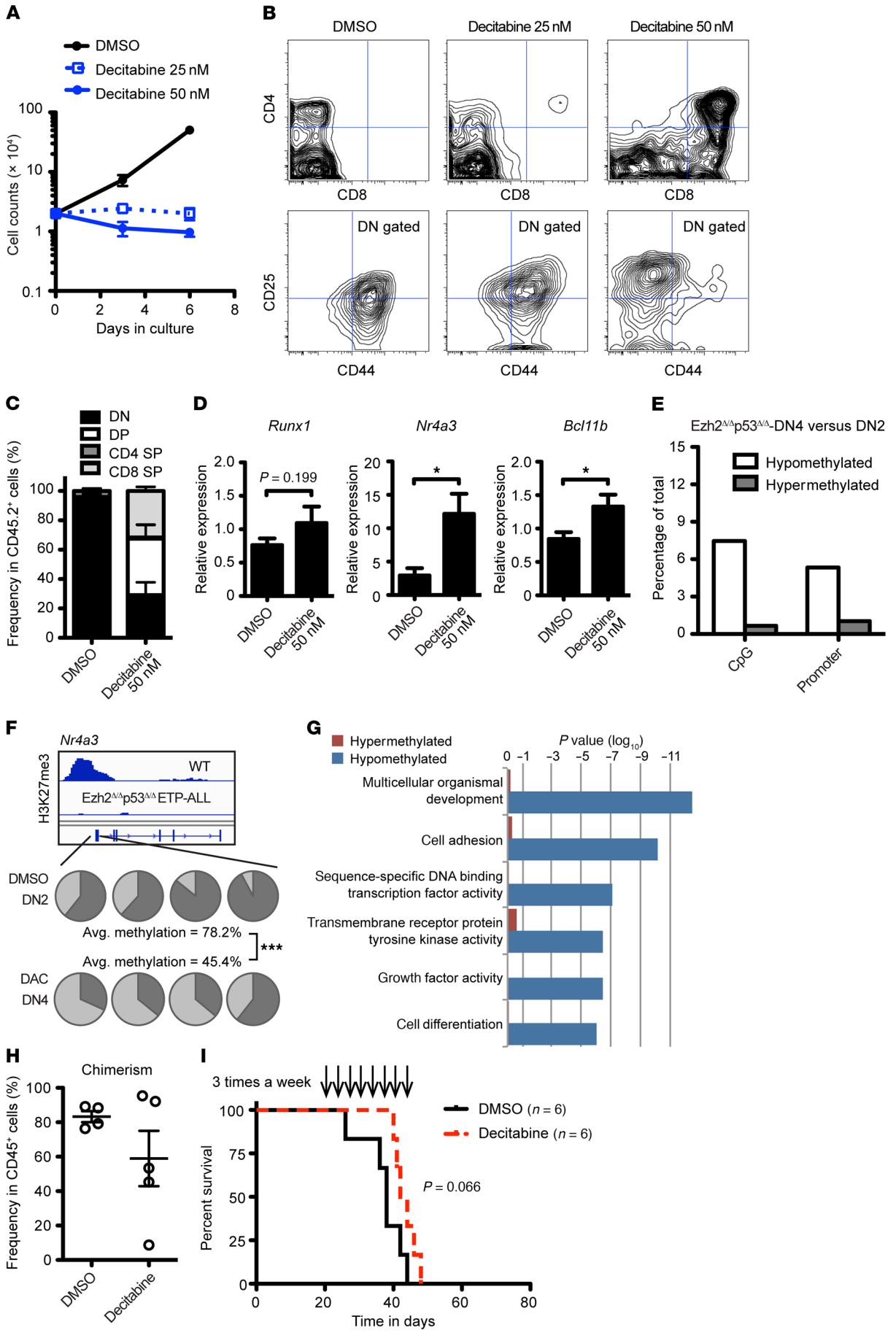
A
DMSO
Decitabine 25 nM
Decitabine 50 nM
Cell counts (× 10⁴)
Days in culture
B
DMSO
Decitabine 25 nM
Decitabine 50 nM
CD4
CD8
DN gated
CD25
CD44
C
DN
DP
CD4 SP
CD8 SP
Frequency in CD45.2⁺ cells (%)
DMSO
Decitabine 50 nM
D
Runx1
Nr4a3
Bcl11b
P = 0.199
Relative expression
E
Ezh2Δ/Δp53Δ/Δ-DN4 versus DN2
Hypomethylated
Hypermethylated
Percentage of total
CpG
Promoter
F
Nr4a3
H3K27me3
WT
Ezh2Δ/Δp53Δ/Δ ETP-ALL
DMSO DN2
Avg. methylation = 78.2%
***
Avg. methylation = 45.4%
DAC DN4
G
Hypermethylated
Hypomethylated
P value (log10)
Multicellular organismal development
Cell adhesion
Sequence-specific DNA binding transcription factor activity
Transmembrane receptor protein tyrosine kinase activity
Growth factor activity
Cell differentiation
H
Chimerism
Frequency in CD45⁺ cells (%)
DMSO
Decitabine
I
3 times a week
DMSO (n = 6)
Decitabine (n = 6)
P = 0.066
Percent survival
Time in days

Figure 7. Aberrant DNA hypermethylation sensitized ETP-ALL cells to a DNA hypomethylating agent. (**A**) Total cell counts of control (black line) and DAC-treated (25 nM, blue broken line; 50 nM, blue line) Ezh2$^{\Delta/\Delta}$ p53$^{\Delta/\Delta}$ ETP-ALL cells monitored for 6 days in the culture (n = 3). Data are representative of 3 independent experiments. (**B**) Representative flow cytometric profiles of CD4 and CD8 expression (top) and CD44 and CD25 expression in CD4$^-$CD8$^-$ DN cells (bottom) on day 6 of the culture in **A**. (**C**) Proportions of CD4$^+$CD8$^+$ DP cells, CD4 SP cells, CD8 SP cells, and CD4$^-$CD8$^-$ DN cells in control and DAC-treated (50 nM) cultures on day 6 (n = 4–5). (**D**) Quantitative RT-PCR analysis of the expression of *Runx1*, *Bcl11b*, and *Nr4a3* in purified DN2 cells harvested from control and ETP-ALL cells treated with 50 nM DAC on day 3 of the culture (n = 6–9). (**E**) Numbers of hypo- and hyper-DMRs at CGIs and promoters in DAC-induced Ezh2$^{\Delta/\Delta}$p53$^{\Delta/\Delta}$ leukemic DN4 cells relative to DMSO-induced Ezh2$^{\Delta/\Delta}$p53$^{\Delta/\Delta}$ leukemic DN2 cells. (**F**) ChIP-seq view of H3K27me3 levels at the *Nr4a3* locus in WT and Ezh2$^{\Delta/\Delta}$ p53$^{\Delta/\Delta}$ leukemic DN1 cells and RRBS data of DNA methylation at the *Nr4a3* locus in Ezh2$^{\Delta/\Delta}$p53$^{\Delta/\Delta}$ leukemic DN2 cells and DAC-induced Ezh2$^{\Delta/\Delta}$ p53$^{\Delta/\Delta}$ leukemic DN4 cells. ***P < 0.001, Student's t test. (**G**) GO biological process gene sets enriched in hyper-DMRs (red bars) and hypo-DMRs (blue bars). (**H**) Chimerism of CD45.2$^+$ cells in the PB cells of DMSO-treated and DAC-treated (0.2 mg/kg, 3 times a week) Ezh2$^{\Delta/\Delta}$p53$^{\Delta/\Delta}$ leukemic mice 3 weeks after the completion of the treatment (n = 4–5). (**I**) Longer median survival of DAC-treated Ezh2$^{\Delta/\Delta}$p53$^{\Delta/\Delta}$ leukemic mice compared with DMSO-treated mice (n = 6). Representative data of the 2 independent experiments are shown. P value is by log-rank test.

Western blotting. The antibodies used for Western blotting were as follows: anti-H3K27me3 (07449, Merck Millipore) and anti-H3 (ab1791, Abcam).

Quantitative RT-PCR. Quantitative RT-PCR was performed on a StepOnePlus Real-Time PCR System (Life Technologies) by using SYBR Premix Ex TaqII (Takara) or FastStart Universal Probe Master (Roche) with the Universal ProbeLibrary (Roche). Primer sequences with Universal ProbeLibrary (Roche) numbers are as follows: *Ezh2* (forward, CCAGACTGGTGAAGAGTTGTTTT; reverse, CAAGGGATTTCCATTTCTCG; no. 105); *p53* (forward, ATGCCCATGCTACAGAGGAG; reverse, AGACTGGCCCTTCTTGGTCT; no. 94); *p16^{Ink4a}* (forward, AATCTCCGCGAGGAAAGC; reverse, GTCTGCAGCGGACTCCAT; no. 91); *p19^{ARF}* (forward, GGGTTTTCTTGGTGAAGTTCG; reverse, TTGCCCATCATCATCACCT; no. 106); *Nr4a3* (forward, GTGTCGGGATGGTTAAGGAA; reverse, CCTGTTGTAGTGGGCTCTTTG; no. 97); *Runx1* (forward, CTCCGTGCTACCCACTCACT; reverse, ATGACGGTGACCAGAGTGC; no. 77); *Bcl11b* (forward, TGGATGCCAGTGTGAGTTGT; reverse, GCTGCTTGCATGTTGTGC; no. 97); *Ptcra* (forward, TCAGGTGTCAGGCTCTACCA; reverse, GCCTTCCATCTACCAGCAGT; no. 106); *Hlf* (forward, CTACGGCGTGCTCAGGTC; reverse, TCCTTTGTCTTTTTCTTTACTAAATGC; no. 67); *Hoxa10* (forward, CCTTCAGAAAACAGTAAAGCTTCG; reverse, AAGGGCAGCGTTTCTTCC; no. 100); *Dnmt1* (forward, CATGGTCTTCCCCCACTCTCTTG; reverse, ACAGAACAGCTCTGAACGAGACC); *Dnmt3a* (forward, GAAACTAAGGTGCTGGGGACTGG; reverse, CCTTAGTTCTGTGACCCTGGTGC); *Dnmt3b* (forward, TTGTGCCAGACCTTGGAAACCTC; reverse, AAAGAAGGCCCTGGATTTGGTCC); and *Gapdh* (forward, ATGACATCAAGAAGGTGGTGAAG; reverse, TCCTTGGAGGCCATGTAGG). All data are presented as relative expression levels normalized to *Gapdh* expression.

Microarray and data analyses. Total RNA was extracted from approximately 1 × 10^5 pooled cells from 5 to 10 mice using an RNeasy Plus Mini Kit (QIAGEN). Twenty nanograms of total RNA was mixed with spike-in controls using an Agilent One Color Spike Mix Kit, amplified, and labeled with Cyanine 3 using a Low Input Quick Amp Labeling Kit (Agilent) according to the manufacturer's instructions. A microarray analysis using a SurePrint G3 Mouse GE Microarray 8x60K Kit (Agilent) was performed according to the manufacturer's instructions. Hierarchical clustering and principal component analyses based on total gene expression were performed using WebMeV (Multiple Experiment Viewer) software.

RRBS. RRBS was performed as previously described (9, 24).

ChIP sequencing. ChIP assays were performed as previously described (8). Briefly, 1 × 10^5 pooled DN1 cells were used for each immunoprecipitation reaction with an anti-H3K27me3 (Merck Millipore, 07449) antibody.

Sequencing data analysis. The ChIP-seq signal was quantified as the total number of reads per million. In order to evaluate the histone modification mark of each gene, normalized tag numbers in the region from 2 kb upstream to 2 kb downstream of the TSS were counted and divided by the tag number of the corresponding input. The reads per kilobase of transcripts per million mapped reads (RPKM) values of the sequenced reads were calculated every 5,000 bp bin with a shifting size of 500 bp using bedtools to be visualized with the Integrative Genomics Viewer (IGV) genome browser. The read numbers of the immunoprecipitated samples were then normalized by subtracting the RPKM values of the input samples in each bin and converted to a BigWig file using the wigToBigWig tool. The supercomputing resource was provided by the Human Genome Center, Institute of Medical Science, University of Tokyo (http://sc.hgc.jp/shirokane.html).

PCR analysis of TCR-β gene rearrangement. Genomic DNA was extracted from approximately 1 × 10^5 DN2 cells. Extracted DNA was amplified by PCR with primers of Dβ-1.1, extension GAGGAGCAGCTTATCTGGTG, and Jβ-1.7, extension AAGGGACGACTCTGTCTTAC, by using T100 Thermal Cycler (Bio-Rad). A PCR product of the first amplification was subjected to a second PCR with nested primers of Dβ-1.1, internal GGTAGACCTATGGGAGGGC, and Jβ-1.7, internal ACCATGGTCATCCAACACAG, as previously described (44).

Statistics. All statistical tests were performed using GraphPad Prism version 7 (GraphPad Software). The significance of differences was measured by an unpaired 2-tailed Student's t test or Mann-Whitney nonparametric test. A P value of less than 0.05 was considered significant.

Study approval. All animal studies were reviewed and approved by the Review Boards for Animal Experiments of Chiba University (approval ID: 30-56) and Kumamoto University (approval ID: A 30-006).

Accession codes. ChIP sequencing and RRBS data were deposited in the DNA Data Bank of Japan (DDBJ PRJDB5585 and PRJDB6937). All original microarray data were deposited in the NCBI's Gene Expression Omnibus database (GEO GSE95655).

Author contributions

CW performed experiments and analyzed results. MO analyzed results. DS, HM, SK, KA, YNT, SK, JM, MMK, TNY, and JB performed experiments. TN provided reagents. AK analyzed results. AI and GS designed the research, performed experiments, analyzed results, and wrote the manuscript.

Acknowledgments

The authors thank the members of the Iwama Laboratory for their discussions during the preparation of this manuscript. The authors thank Haruhiko Koseki and Anton Berns for kindly pro-

viding *Ezh2* and *p53* conditional knockout mice, respectively, and Hiroshi Kawamoto for kindly providing TSt-4/DLL4 cells. The supercomputing resource was provided by the Human Genome Center (Institute of Medical Science, University of Tokyo). This work was supported in part by Grants-in-Aid for Scientific Research (nos. 15H02544, 25130702, 26461396, and 16KT0113), Scientific Research on Innovative Areas Cell Fate (no. 22118004) and Stem Cell Aging and Disease (no. 26115002) from the Ministry of Education, Culture, Sports, Science and Technology, Japan, a Program of Higher-Level Talents of Inner Mongolia University award (to Changshan Wang), and the National Natural Science Foundation of China (no. 81660024).

Address correspondence to: Goro Sashida, 2-2-1 Honjo, Chuo-ku, Kumamoto 860-0811, Japan. Phone: 81.96.373.6827; Email: sashidag@kumamoto-u.ac.jp. Or to: Atsushi Iwama, 4-6-1 Shirokanedai, Minato-ku, Tokyo 108-8639, Japan. Phone: 81.3.6409.2180; Email: 03aiwama@ims.u-tokyo.ac.jp.

1. Coustan-Smith E, et al. Early T-cell precursor leukaemia: a subtype of very high-risk acute lymphoblastic leukaemia. *Lancet Oncol*. 2009;10(2):147–156.
2. Zhang J, et al. The genetic basis of early T-cell precursor acute lymphoblastic leukaemia. *Nature*. 2012;481(7380):157–163.
3. Mochizuki-Kashio M, et al. Dependency on the polycomb gene Ezh2 distinguishes fetal from adult hematopoietic stem cells. *Blood*. 2011;118(25):6553–6561.
4. Xie H, et al. Polycomb repressive complex 2 regulates normal hematopoietic stem cell function in a developmental-stage-specific manner. *Cell Stem Cell*. 2014;14(1):68–80.
5. Shih AH, Abdel-Wahab O, Patel JP, Levine RL. The role of mutations in epigenetic regulators in myeloid malignancies. *Nat Rev Cancer*. 2012;12(9):599–612.
6. Iwama A. Polycomb repressive complexes in hematological malignancies. *Blood*. 2017;130(1):23–29.
7. Ntziachristos P, et al. Genetic inactivation of the polycomb repressive complex 2 in T cell acute lymphoblastic leukemia. *Nat Med*. 2012;18(2):298–301.
8. Muto T, et al. Concurrent loss of Ezh2 and Tet2 cooperates in the pathogenesis of myelodysplastic disorders. *J Exp Med*. 2013;210(12):2627–2639.
9. Sashida G, et al. Ezh2 loss promotes development of myelodysplastic syndrome but attenuates its predisposition to leukaemic transformation. *Nat Commun*. 2014;5:4177.
10. Sashida G, et al. The loss of Ezh2 drives the pathogenesis of myelofibrosis and sensitizes tumor-initiating cells to bromodomain inhibition. *J Exp Med*. 2016;213(8):1459–1477.
11. Mochizuki-Kashio M, et al. Ezh2 loss in hematopoietic stem cells predisposes mice to develop heterogeneous malignancies in an Ezh1-dependent manner. *Blood*. 2015;126(10):1172–1183.
12. Simon C, et al. A key role for EZH2 and associated genes in mouse and human adult T-cell acute leukemia. *Genes Dev*. 2012;26(7):651–656.
13. Danis E, et al. Ezh2 controls an early hematopoietic program and growth and survival signaling in early T cell precursor acute lymphoblastic leukemia. *Cell Rep*. 2016;14(8):1953–1965.
14. Donehower LA, et al. Mice deficient for p53 are developmentally normal but susceptible to spontaneous tumours. *Nature*. 1992;356(6366):215–221.
15. Grossmann V, et al. The molecular profile of adult T-cell acute lymphoblastic leukemia: mutations in RUNX1 and DNMT3A are associated with poor prognosis in T-ALL. *Genes Chromosomes Cancer*. 2013;52(4):410–422.
16. Seki M, et al. Recurrent SPI1 (PU.1) fusions in high-risk pediatric T cell acute lymphoblastic leukemia. *Nat Genet*. 2017;49(8):1274–1281.
17. Jonkers J, Meuwissen R, van der Gulden H, Peterse H, van der Valk M, Berns A. Synergistic tumor suppressor activity of BRCA2 and p53 in a conditional mouse model for breast cancer. *Nat Genet*. 2001;29(4):418–425.
18. Cheng LE, Chan FK, Cado D, Winoto A. Functional redundancy of the Nur77 and Nor-1 orphan steroid receptors in T-cell apoptosis. *EMBO J*. 1997;16(8):1865–1875.
19. Belyaev NN, Biró J, Athanasakis D, Fernandez-Reyes D, Potocnik AJ. Global transcriptional analysis of primitive thymocytes reveals accelerated dynamics of T cell specification in fetal stages. *Immunogenetics*. 2012;64(8):591–604.
20. Ikawa T, et al. An essential developmental checkpoint for production of the T cell lineage. *Science*. 2010;329(5987):93–96.
21. Li L, Leid M, Rothenberg EV. An early T cell lineage commitment checkpoint dependent on the transcription factor Bcl11b. *Science*. 2010;329(5987):89–93.
22. Grossmann V, et al. Prognostic relevance of RUNX1 mutations in T-cell acute lymphoblastic leukemia. *Haematologica*. 2011;96(12):1874–1877.
23. Chambers SM, et al. Hematopoietic fingerprints: an expression database of stem cells and their progeny. *Cell Stem Cell*. 2007;1(5):578–591.
24. Hasegawa N, et al. Impact of combinatorial dysfunctions of Tet2 and Ezh2 on the epigenome in the pathogenesis of myelodysplastic syndrome. *Leukemia*. 2017;31(4):861–871.
25. Lister R, et al. Human DNA methylomes at base resolution show widespread epigenomic differences. *Nature*. 2009;462(7271):315–322.
26. Challen GA, et al. Dnmt3a is essential for hematopoietic stem cell differentiation. *Nat Genet*. 2011;44(1):23–31.
27. Morin RD, et al. Somatic mutations altering EZH2 (Tyr641) in follicular and diffuse large B-cell lymphomas of germinal-center origin. *Nat Genet*. 2010;42(2):181–185.
28. Béguelin W, et al. EZH2 is required for germinal center formation and somatic EZH2 mutations promote lymphoid transformation. *Cancer Cell*. 2013;23(5):677–692.
29. Tanaka S, et al. Ezh2 augments leukemogenicity by reinforcing differentiation blockage in acute myeloid leukemia. *Blood*. 2012;120(5):1107–1117.
30. Neff T, et al. Polycomb repressive complex 2 is required for MLL-AF9 leukemia. *Proc Natl Acad Sci U S A*. 2012;109(13):5028–5033.
31. Souroullas GP, et al. An oncogenic Ezh2 mutation induces tumors through global redistribution of histone 3 lysine 27 trimethylation. *Nat Med*. 2016;22(6):632–640.
32. Su IH, et al. Polycomb group protein ezh2 controls actin polymerization and cell signaling. *Cell*. 2005;121(3):425–436.
33. Yui MA, Rothenberg EV. Developmental gene networks: a triathlon on the course to T cell identity. *Nat Rev Immunol*. 2014;14(8):529–545.
34. Rasmussen KD, Helin K. Role of TET enzymes in DNA methylation, development, and cancer. *Genes Dev*. 2016;30(7):733–750.
35. Manzo M, Wirz J, Ambrosi C, Villaseñor R, Roschitzki B, Baubec T. Isoform-specific localization of DNMT3A regulates DNA methylation fidelity at bivalent CpG islands. *EMBO J*. 2017;36(23):3421–3434.
36. Ohm JE, et al. A stem cell-like chromatin pattern may predispose tumor suppressor genes to DNA hypermethylation and heritable silencing. *Nat Genet*. 2007;39(2):237–242.
37. Maegawa S, et al. Age-related epigenetic drift in the pathogenesis of MDS and AML. *Genome Res*. 2014;24(4):580–591.
38. Boulard M, Edwards JR, Bestor TH. FBXL10 protects Polycomb-bound genes from hypermethylation. *Nat Genet*. 2015;47(5):479–485.
39. Zenatti PP, et al. Oncogenic IL7R gain-of-function mutations in childhood T-cell acute lymphoblastic leukemia. *Nat Genet*. 2011;43(10):932–939.
40. Treanor LM, et al. Interleukin-7 receptor mutants initiate early T cell precursor leukemia in murine thymocyte progenitors with multipotent potential. *J Exp Med*. 2014;211(4):701–713.
41. Maude SL, et al. Efficacy of JAK/STAT pathway inhibition in murine xenograft models of early T-cell precursor (ETP) acute lymphoblastic leukemia. *Blood*. 2015;125(11):1759–1767.
42. Hirabayashi Y, et al. Polycomb limits the neurogenic competence of neural precursor cells to promote astrogenic fate transition. *Neuron*. 2009;63(5):600–613.
43. Mishima Y, et al. Histone acetylation mediated by Brd1 is crucial for Cd8 gene activation during early thymocyte development. *Nat Commun*. 2014;5:5872.
44. King AG, Kondo M, Scherer DC, Weissman IL. Lineage infidelity in myeloid cells with TCR gene rearrangement: a latent developmental potential of proT cells revealed by ectopic cytokine receptor signaling. *Proc Natl Acad Sci U S A*. 2002;99(7):4508–4513.